UC Davis
UC Davis Previously Published Works

Title

Width undulation drives flow convergence routing in five flashy ephemeral river types across a dry summer subtropical region

Permalink

https://escholarship.org/uc/item/83s970pw

Journal

Earth Surface Processes and Landforms, 49(6)

ISSN

0197-9337

Authors

Nogueira, Xavier R

Pasternack, Gregory B

Lane, Belize A

et al.

Publication Date

2024-05-01

DOI

10.1002/esp.5805

Copyright Information

This work is made available under the terms of a Creative Commons Attribution License, available at https://creativecommons.org/licenses/by/4.0/

Peer reviewed

RESEARCH ARTICLE

ESPL WILEY

Width undulation drives flow convergence routing in five flashy ephemeral river types across a dry summer subtropical region

Xavier R. Nogueira[1] | Gregory B. Pasternack[1] | Belize A. Lane[2] | Samuel Sandoval-Solis[1]

[1]University of California, Davis, Davis, CA, USA

[2]Utah State University, Logan, UT, USA

Correspondence
Gregory B. Pasternack, University of California, Davis, One Shields Avenue, Davis, CA 95616, USA.
Email: gpast@ucdavis.edu

Abstract

During the last decade, meter-resolution topo-bathymetric digital elevation models (DEMs) have become increasingly utilized within fluvial geomorphology, but most meter-scale geomorphic analyses are done on just one to a few rivers. While such analyses have contributed greatly to our collective understanding of river discharge-topography interactions, which is applicable in both river restoration design and environmental flow regulation contexts, their generalizability across a range of river types remains largely unevaluated. This study assessed the dominance of a single hydro-morphodynamic mechanism, flow convergence routing, in 35 ephemeral rivers divided among five river types in California's South Coast region by answering five questions. Geomorphic covariance structure (GCS) analysis was performed on longitudinal standardized width and standardized, detrended bed elevation spatial series from meter-resolution DEMs. All river types had coherent, multi-scalar structures of longitudinal fluvial topography, implicating a process-morphology link. GCS metrics revealed that landform patterning was consistent with the requirements of the morphodynamic mechanism of flow convergence routing. Thus, that process was found to be a broadly relevant channel altering mechanism among sites, but its relationship with water stage differed between river types. Specifically, river types in unconfined valleys exhibited a strong bankfull width control over base flow bed undulations, with no obvious flood-stage control over bankfull landform patterning. River types in partially confined valleys also exhibited strong bankfull width control over base flow bed undulations, but their bankfull landform patterns appear to have coalesced with coherent width and bed elevation undulations during flood flows. Finally, metrics for confined river types showed that it takes higher magnitude, less frequent floods to set their coherent width and bed elevation undulations, but even these channels do exhibit flow convergence routing when given enough discharge for sufficient duration.

KEYWORDS
ephemeral rivers, flow convergence routing, fluvial geomorphology, geomorphic covariance analysis, river classification

1 | INTRODUCTION

River type classification assumes each assemblage of geomorphic processes produces a characteristic fluvial morphology (Kasprak et al., 2016; Thornbury, 1954). Yet supporting evidence is lacking because of a dearth of studies investigating the relative role of any hydro-morphodynamic process for significantly different river types. For example, is knickpoint migration (or meander migration, freeze–thaw bank erosion, avulsion, flow convergence routing, nonfluvial boulder emplacement, particle queuing, etc.) equally important for plane-bed, riffle-pool, step-pool, cascade, and bedrock river types? Further, is that process of equal importance in any one river type across all discharges? Some insights into these questions arise from river planform pattern classifications that use numerical thresholds to delineate a few broad types (e.g., Eaton et al., 2010), albeit with some skepticism (Carson, 1984). However, such thresholds are typically general variables without specific relation to individual processes and landforms in such classifications.

A key limitation to evaluating how a hydro-morphodynamic process varies among river types has been the lack of sufficiently detailed (i.e., 1-m resolution) topo-bathymetric mapping of rivers to characterize the essential patterns of variability that drive and indicate individual morphodynamic processes. Variability is present in many key factors, such as sediment facies, aquatic and riparian vegetation, large bed elements (including wood, boulder and bedrock features), and topography. One-meter resolution topo-bathymetric digital elevation models (DEMs) are increasingly available and utilized in fluvial geomorphology (Piegay et al., 2015) to describe topography (Notebaert et al., 2009; Scown et al., 2015), segment rivers (Nardini et al., 2020), model two-dimensional (2D) hydraulics (Milan & Schwendel, 2021; Pasternack, 2011; Tonina et al., 2020), classify and map landforms (Cavalli et al., 2008; Clubb et al., 2017), document sedimentary dynamics (Baartman et al., 2013), identify periodic width (W) and detrended bed elevation (Zd) undulations (Brown & Pasternack, 2017; Duffin et al., 2021), and evaluate topography for specific hydro-morphodynamic mechanisms (Pasternack et al., 2018a, 2018b; Pasternack et al., 2021).

Although novel methods for mapping topographic variability are being developed and piloted for flumes and ideal testbed sites (e.g., Adams, 2020; Mahdade et al., 2018), the financial expense and labor involved as well as the requirement to manually specify algorithm parameters for each river has hindered meter-scale DEM analyses of variability and associated geomorphic processes to only one or a few full-scale river reaches as of yet. Further, many fluvial processes are only explored in a single river type, such as "velocity-reversal" studies of riffle-pool rivers (Carling, 1991) and lateral migration studies in meandering rivers (e.g. Motta et al., 2012). As a result, there is a paucity of scientific meta-analysis and sufficiently automated procedures to analyze and compare a large sample of significantly different river reaches at one time to draw statistically significant, generalizable geomorphic conclusions using consistent methods. The broad scientific question addressed in this article remains: how does a single hydro-morphodynamic process vary among a diversity of river types?

This study aimed to answer this question at the regional scale for a single hydro-morphodynamic mechanism involving topographic variability–flow convergence routing (Jackson et al., 2015; MacWilliams et al., 2006). While hardly comprehensive of global possibilities, the study still is notable for its analysis of 35 river reaches spanning the five flashy ephemeral river types found in California's dry summer subtropical South Coast region (Figure 1). To achieve such a breadth and depth of inquiry using a rigorous experimental design following the scientific method necessitates building on state-of-the-art theory and methods arising from research about flow convergence routing and geomorphic covariance structures (GCS). A primer on these topics is provided in the second section of the article along with a literature review about flashy ephemeral river hydrogeomorphology.

With that foundation, the study addresses the broad scientific question by establishing two research objectives, each with specific, tractable questions (five total) about the hydrogeomorphic process (Figure 2). In turn, testable hypotheses were itemized by key geomorphic variables governing river type, such as valley confinement. Full explanations of the hypotheses stated in Figure 2 are provided in the corresponding first section of the Supplementary Material file.

Objective 1 (O1) assessed the degree to which active channel morphology at three key water stages (baseflow, bankfull, and a flood stage, per the fifth subsection of the fourth section of this article) is consistent with flow convergence routing acting as a dominant hydro-morphodynamic mechanism. Three questions (O1a, O1b, O1c) explored differences between river type and water stage using longitudinal topographic deviations as expressed by standardized width (Ws) and detrended, standardized bed elevation (Zs) series. Such differences were interpreted in relation to the particular pattern of topographic nonuniformity required for flow convergence routing to drive morphodynamics (i.e., positive GCS between Ws and Zs).

Objective 2 (O2) aimed to move beyond typical fluvial research where the landforms and morphodynamics of a given channel dimension are understood by considering drivers for that same dimension. For example, studies of the bankfull channel often focus on hydro-morphodynamics in the bankfull channel (e.g., Bayat et al., 2017). That is a uni-scalar mindset. Yet in nature, a wide, deep "pool" section of the bankfull channel could be a product of a valley wall bedrock outcrop that constricts flood flows, increasing flow velocity and therefore inducing local scour. O2 instead investigated the extent to which South Coast ephemeral river channel bed elevation undulations (O2a) and landforms (O2b) are a product of hydro-morphodynamics driven by larger scales of topography. This is critical because flow convergence routing theory (see second subsection of the second section of this article) dictates that it may take stronger forces than can be produced within a given channel dimension to change and control a channel at that dimension, ceteris paribus. Therefore, resilient low-flow channel dimensions may be maintained by patterns of topographic nonuniformity at higher water stages capable of making channel alterations. Theoretically, a similar relationship between bankfull and flood-stage channel dimensions could also exist but has been hardly studied. In South Coast ephemeral rivers with their characteristic sporadic but intense flood flows, it is possible that very infrequent discharges are the dominant driver of lower water stage channel morphology. On the other hand, bankfull flows are likely to be morphologically relevant themselves and could potentially rework, and obscure, the channel alterations left by flood flows.

2 | ESSENTIAL CONCEPTS

Flow convergence routing (MacWilliams et al., 2006) and GCS (Brown & Pasternack, 2014) theories are young, though they
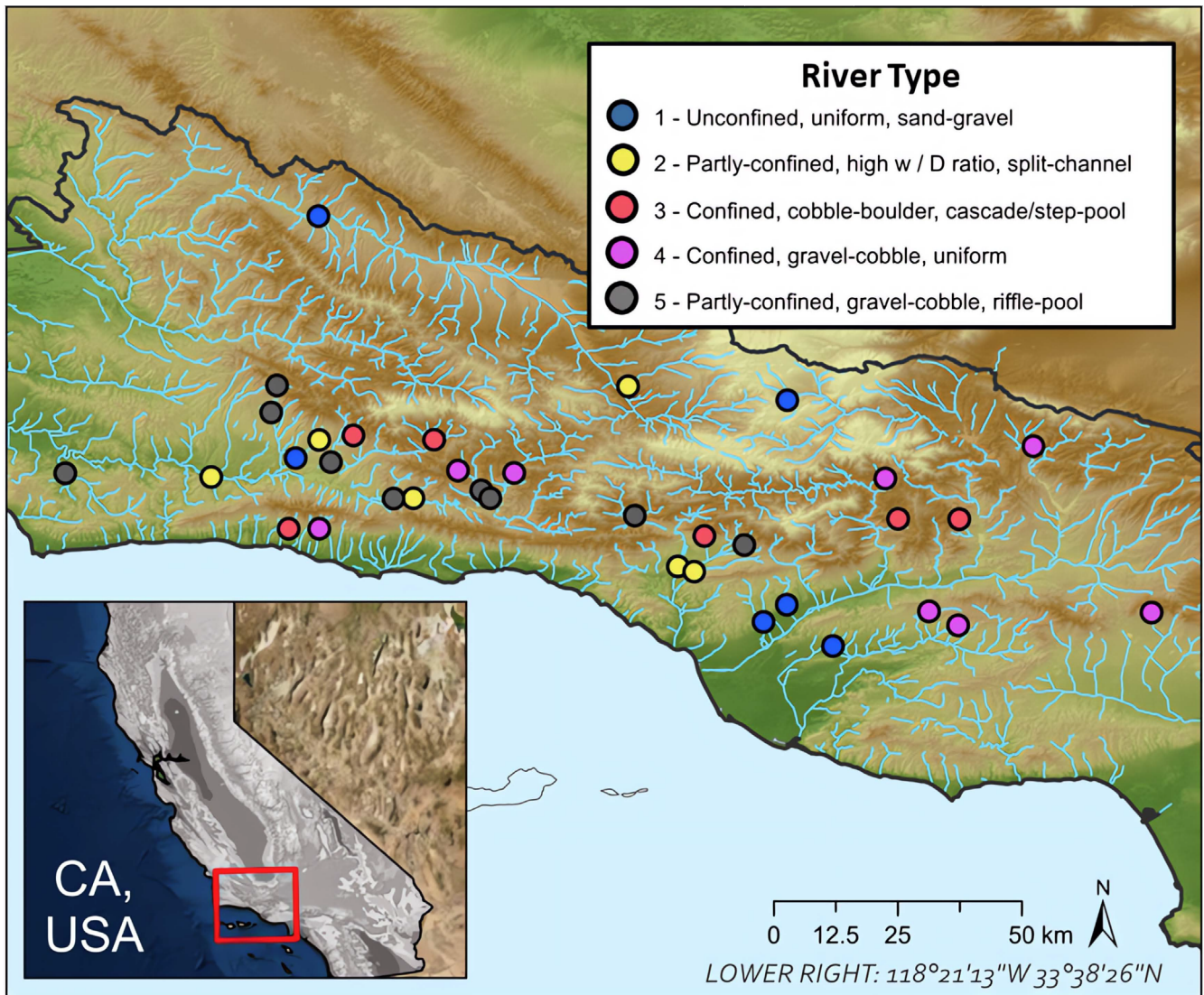
FIGURE 1 Map of the south coast showing all sampled river reaches color coded by river type.

significantly expand upon decades of prior ideas (e.g., Keller, 1971; Kieffer, 1985; Richards, 1976). A key difference from the classic "velocity reversal" theory that is flow convergence routing can occur in any river type, if there are longitudinal differences in cross-sectional area, whereas velocity reversals are considered for just riffle-pool river types. Despite the growing citations and subsequent articles building on the theories and method, these concepts are still new to many people. Therefore, a brief review of their essential theory, methods, and scientific discoveries is provided herein. Because this study applies these to flashy ephemeral rivers, it is also necessary to summarize this unique hydrogeomorphic setting, which is of growing importance to understand river ecosystem and water-supply resilience under climate change (McJannet et al., 2014).

2.1 | Ephemeral rivers

Flashy ephemeral river hydrology involves short, high-intensity rainfall events that drive the largest annual discharges but otherwise have little to no flow between such events (Bull et al., 2000; Priddy & Clarke, 2020). Similarly, intermittent rivers are seasonally ephemeral,

with groundwater contributing to baseflow during the wet season. Together, ephemeral and intermittent rivers drain over half the world's land surface and are most common in arid, semiarid, and Mediterranean regions (Datry et al., 2017). For simplicity, we conceptually group intermittent and flashy ephemeral stream hydrology and henceforth refer to both as "ephemeral".

Ephemeral rivers have precipitation thresholds for channel flow, as opposed to precipitation contributing to a perennial baseflow. The thresholds vary with sediment size, bedrock geology, river type, valley confinement, and vegetation (Hooke, 2016). The spatial heterogeneity of these variables often results in ephemeral rivers having more diverse annual flow regimes than perennial rivers within a given climatic setting (Hooke, 2016; Merritt et al., 2021).

Summarizing ephemeral river geomorphology is difficult; their fluvial processes and morphologies are diverse, spanning a wide variety of environmental settings globally. While many ephemeral river processes and channel forms are analogous to perennial rivers, others are quite distinct (Datry et al., 2017). Climate is one variable affecting channel morphology; in arid environments, with lower clay content and less-dense riparian vegetation, loosely consolidated channel banks promote wide split-channel/braided morphologies (Powell, 2009).
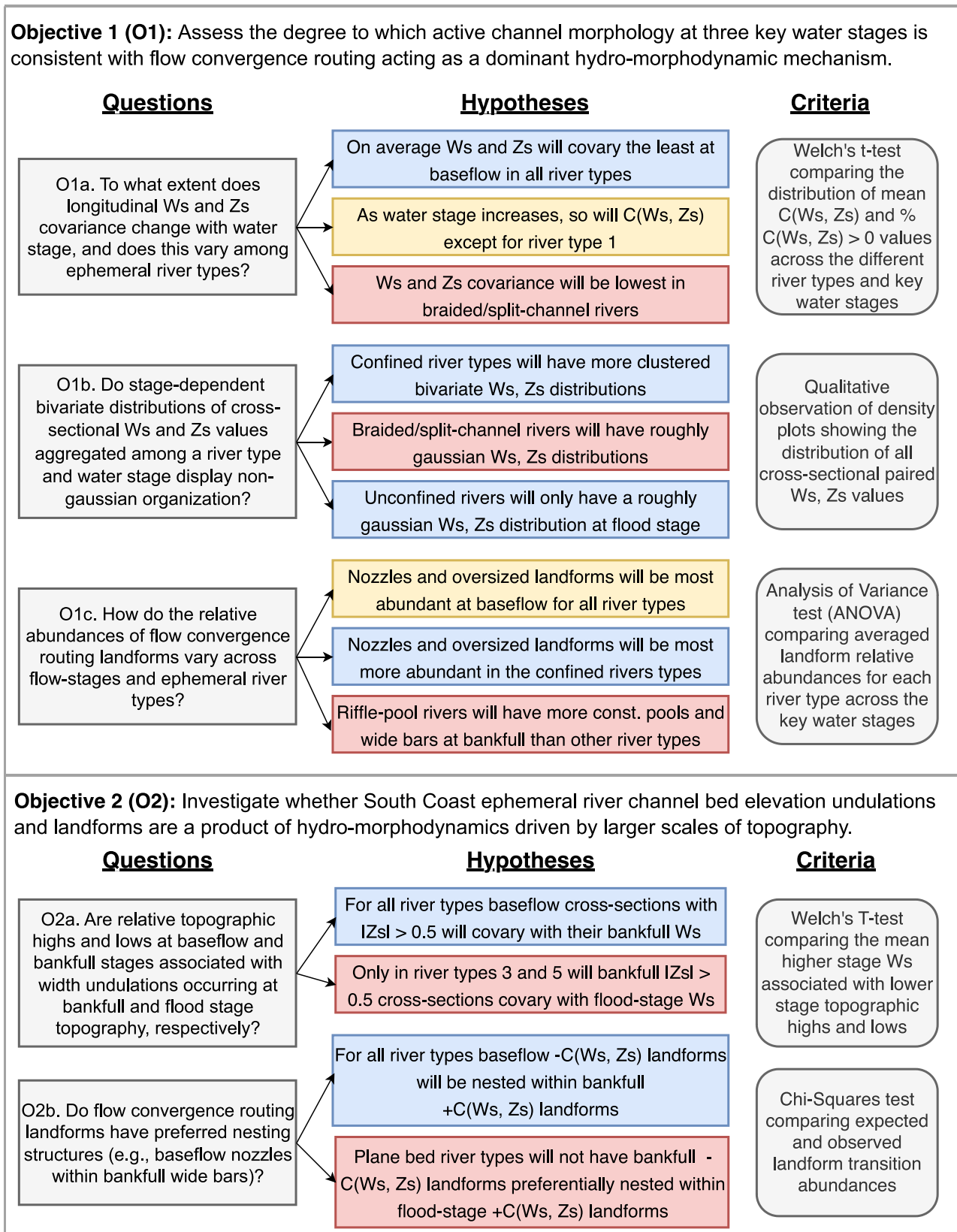
Objective 1 (O1): Assess the degree to which active channel morphology at three key water stages is consistent with flow convergence routing acting as a dominant hydro-morphodynamic mechanism.

Questions

Hypotheses

Criteria

O1a. To what extent does longitudinal Ws and Zs covariance change with water stage, and does this vary among ephemeral river types?

On average Ws and Zs will covary the least at baseflow in all river types

As water stage increases, so will C(Ws, Zs) except for river type 1

Ws and Zs covariance will be lowest in braided/split-channel rivers

Welch's t-test comparing the distribution of mean C(Ws, Zs) and % C(Ws, Zs) > 0 values across the different river types and key water stages

O1b. Do stage-dependent bivariate distributions of cross-sectional Ws and Zs values aggregated among a river type and water stage display non-gaussian organization?

Confined river types will have more clustered bivariate Ws, Zs distributions

Braided/split-channel rivers will have roughly gaussian Ws, Zs distributions

Unconfined rivers will only have a roughly gaussian Ws, Zs distribution at flood stage

Qualitative observation of density plots showing the distribution of all cross-sectional paired Ws, Zs values

O1c. How do the relative abundances of flow convergence routing landforms vary across flow-stages and ephemeral river types?

Nozzles and oversized landforms will be most abundant at baseflow for all river types

Nozzles and oversized landforms will be most more abundant in the confined rivers types

Riffle-pool rivers will have more const. pools and wide bars at bankfull than other river types

Analysis of Variance test (ANOVA) comparing averaged landform relative abundances for each river type across the key water stages

Objective 2 (O2): Investigate whether South Coast ephemeral river channel bed elevation undulations and landforms are a product of hydro-morphodynamics driven by larger scales of topography.

Questions

Hypotheses

Criteria

O2a. Are relative topographic highs and lows at baseflow and bankfull stages associated with width undulations occurring at bankfull and flood stage topography, respectively?

For all river types baseflow cross-sections with |Zs| > 0.5 will covary with their bankfull Ws

Only in river types 3 and 5 will bankfull |Zs| > 0.5 cross-sections covary with flood-stage Ws

Welch's T-test comparing the mean higher stage Ws associated with lower stage topographic highs and lows

O2b. Do flow convergence routing landforms have preferred nesting structures (e.g., baseflow nozzles within bankfull wide bars)?

For all river types baseflow -C(Ws, Zs) landforms will be nested within bankfull +C(Ws, Zs) landforms

Plane bed river types will not have bankfull -C(Ws, Zs) landforms preferentially nested within flood-stage +C(Ws, Zs) landforms

Chi-Squares test comparing expected and observed landform transition abundances

FIGURE 2 A flow chart displaying both study objectives, their associated questions, as well as our question specific hypotheses and testing criteria. Hypotheses are color coded in relation to our study's findings; blue = hypothesis was supported, yellow = hypothesis was largely supported but with some qualifications, and red = hypothesis was rejected.

Further, infiltration and evaporative transmission losses in ephemeral rivers can decrease sediment carrying capacity more than downstream slope reductions alone, therefore factors such as substrate infiltration rates and evaporative potential post-precipitation event can significantly contribute to network scale depositional patterns (Billi et al., 2018; Datry et al., 2017). Network transmission losses within ephemeral streams inhibit downstream transport of fine-grained sediments relative to that typical in perennial systems, contributing to

poorly sorted channel sediments (Powell et al., 2001). In addition, low flood frequency in ephemeral rivers enables high rates of vegetation encroachment into the channel. Therefore, precipitation event recurrence partly controls channel hydraulic roughness, which in turn affects scour/deposition patterns (Hooke, 2016; Segura-Beltran & Sanchis-Ibor, 2013).

Like perennial rivers, ephemeral rivers organize in a network of diverse river types. In the dry-summer subtropical climate, longitudinal position within an ephemeral stream network is the primary factor controlling channel morphology. As described by Datry et al. (2017), distinct morphologies are seen in the production, transfer, and deposition zones of an ephemeral stream network. The production zone, describing upland areas dominated by hillslope erosion, tend to have ephemeral river morphologies characterized by small, steep, single-thread channels with poorly sorted sediments and low width-depth ratios (Datry et al., 2017; Wohl & Pearthree, 1991). Upland channel morphology can appear quasi-stable between stochastic and quasi-periodic disturbances, such as El Niño/La Niña-driven wildfires and floods during anomalously strong years. Rare disturbances, especially when arriving in a fire-flood sequence, dominate sediment flux and channel evolution (Gray, Pasternack, Watson, Warrick, & Goni, 2015; Warrick et al., 2012).

Ephemeral rivers are ideal for automated geomorphic investigation because dry season airborne LiDAR provides complete river-corridor and channel-bottom coverage. Fluvial bathymetric LiDAR data availability in perennial rivers is limited because of turbidity, depth, forest cover, and other constraints (Lague & Feldmann, 2020), and this has previously prevented comparative analysis among many river corridors in a single study. Focusing on ephemeral rivers affords such unprecedented spatial scale of analysis. However, one limitation is that study findings must be interpreted within the context of established and emerging geomorphological differences between ephemeral and perennial rivers (Tooth, 2000). It may be that shorter duration flooding and faster hydrograph recession in ephemeral rivers better preserves landform changes induced by peak flows, which would make a greater extent of fluvial landforms mapped by LiDAR more representative of a narrower range of discharges during an event.

2.2 | Flow convergence routing

The topography of a river corridor is largely controlled by hydro-morphodynamic processes driven by temporally variable discharge and sediment supply interacting with spatially heterogeneous fluvial topography (De Almeida & Rodríguez, 2012). The nature of this interaction can vary but has been studied as an assemblage of geomorphic processes that are linked to observed patterns of scouring and deposition (Wyrick & Pasternack, 2016). One such morphodynamic mechanism is "flow convergence routing", which is broadly characterized by significant longitudinal topographic heterogeneity, inundated to various degrees depending on discharge, driving stage-dependent, non-uniform patterns of lateral and vertical flow funneling (i.e., convergence and divergence) resulting in longitudinal patterning of deposition and scour. Flow convergence routing is not limited to riffle-pool river types, and it could be present in a wide diversity of types, working together with other morphodynamic processes.

According to flow convergence routing theory (Jackson et al., 2015; MacWilliams et al., 2006), all else equal for a constant discharge down a river, a smaller cross-sectional area (i.e., geometric constriction) has a higher potential to scour and route sediment through it because mass and momentum conservation dictate higher velocity and flow streamlines coming together. Vice-versa, a large cross-sectional area causes momentum dispersion via streamline divergence, decreasing velocity and thereby increasing deposition. Further, the locations of small and large cross-sectional areas shift along the river corridor with water stage because complex non-uniform river topography operates over different discharge ranges (Brown et al., 2015; Pasternack et al., 2018a, 2018b). The velocity at any expansion or constriction may become low or high enough, respectively, at a specific discharge to affect sediment deposition or scour, respectively. For low discharge, there could be intense but highly localized scour at a highly constricted "nozzle", but insufficient sediment transport capacity to route that material further downstream. As a result, this relationship between cross-sectional geometry and fluvial hydro-morphodynamics is expected to only control systemic landform patterning at the range of morphologically relevant discharges not only capable of mobilizing bedload but really transforming the terrain (Caamaño et al., 2009; Pasternack et al., 2018b; Pasternack et al., 2021).

Recent studies of a few river segments have identified a threshold water stage above which landform structure is organized to be freely self-maintaining predominantly (but not exclusively) via flow convergence routing morphodynamics. For wide gravel/cobble lowland rivers and confined, steep mountain rivers, the threshold is identifiable in landform metrics for the cross-sectional area inundated by a discharge or stage one to two times that of bankfull (Pasternack et al., 2021). However, the channel-forming flow causing that change appears to be significantly greater (Pasternack et al., 2018b, 2021). In other words, a flow just inundating the bankfull channel identifies bankfull landforms but appears to have insufficient shear stress to substantially change them. Meanwhile, a large flood inundating the width of a river corridor could really force bankfull landforms to conform to imposed hydraulics, while any peripheral floodplain, terraces, and other features might not be subject to enough shear stress for them to change.

2.3 | Geomorphic covariance structure (GCS) and landforms

A foundational concept in geomorphology states that each geomorphic process leaves its hallmark indicators on the Earth's surface, and in doing so produces a characteristic landform pattern (Thornbury, 1954). On this basis, many geomorphic methods and an extensive literature involve inspection of landforms to infer and quantify processes (Passalacqua et al., 2015). Yet, all such methods have a critical assumption: nothing of geomorphic significance has transpired between the occurrence of the process of inquiry and the time of scientific observation. This assumption hinges on the aggressiveness of the disturbance regime present and the resistance of the terrain to change. For example, beach landforms composed of unconsolidated, rounded sand grains may adjust every day, whereas continental valleys carved by vast glacial outburst floods might only adjust every 10^5 years. Consequently, to observe a process-landform correspondence, an observer must match the spatial scale of observation to that of the process (e.g., Wilson & Goodbred, 2015), mindful of the time

scale characterizing the disturbance regime (Gray, Pasternack, Watson, Warrick, & Goni, 2015; Gray, Pasternack, Watson, Warrick, & Goñi, 2015). Inevitably, the occurrence of repetitions of the same process through time and the co-occurrence of multiple processes make geomorphological reconstructions more difficult, but many studies have observed direct correspondences between processes and landforms (e.g., Perignon et al., 2020; Sawyer et al., 2010) corroborating the practice, while still necessitating vigilance.

One key attribute of flow convergence routing theory is its ability to conceptually link a hydro-morphodynamic mechanism to quantifiable fluvial topographic patterning, allowing its dominance as a fluvial process at a given discharge to be directly investigated from inundated topography alone. This contrasts most other fluvial hydro-morphodynamic analyses that attempt to use computed bed shear stress as an intermediary to explain topographic patterning. Bed shear stress is important for evaluating sediment entrainment and load (e.g., Fernandez Luque & Van Beek, 1976) as well as minor channel bed adjustments (e.g., Petit, 187) but has not been proven useful for understanding wholesale fluvial landform re-organization. Some approaches to computing bed shear stress have unacceptable assumptions considering significant natural river nonuniformity (White et al., 2010) and neglect of flood duration as a critical determinant (Diplas et al., 2008). Others involve time consuming and computationally intensive numerical modeling. All bed shear stress approaches yield estimates with high uncertainty (Yager et al., 2018).

One strategy to unlock the process-morphology connection where landform snapshots are diagnostic of processes is to use the theory of GCS analysis first described by Brown & Pasternack (2014) and Brown et al. (2014). Subsequent studies further articulated GCS concepts, methods, and results relevant for the current study, as summarized in the following overview. Detailed concepts and methods are left for readers to seek out especially in Pasternack et al. (2018a, 2021). There is also an online, free introductory video series of five presentations explaining GCS theory and its findings prior to this study: (1) https://youtu.be/VSMK72FbTfI, (2) https://youtu.be/mZT3wbRAZZ4, (3) https://youtu.be/tr82mvR-5kY, (4) https://youtu.be/yssqRndHleQ, and (5) https://youtu.be/fp1Nag4kN7s.

Many fluvial variables can be quantified as they vary longitudinally downstream. A GCS is simply the linked bivariate pattern of any two of them. A GCS is not a summary statistic, such as covariance; it is the complete bivariate spatial series. The bivariate linkage of any GCS can be made using a decision tree or a mathematical operator such as the product- whatever helps reveal hydro-geomorphic processes. The GCS between Ws and Zs (an inverse proxy for depth) has been shown to accurately predict the hydrodynamic mechanism involved in flow convergence routing (Pasternack et al., 2018b).

A flow chart summarizes the flow convergence routing morphodynamic implications of the different Ws, Zs covariance relationships possible at any given water stage (Figure 3). When Ws and Zs are both either positive or negative at discharges capable of sediment routing and geomorphic change, then the conditions for flow convergent routing will be present and it will be capable of maintaining in-phase bed and width undulations, such as riffle-pool sequencing in an alluvial river. Other process may be occurring at the same time, but these conditions are diagnostic of flow convergence routing (Pasternack et al., 2018b). One simple metric used to capture this outcome is the covariance product of Ws and Zs, C (Ws, Zs), which is calculated across the complete bivariate spatial series. Flow convergence routing theory anticipates that Ws and Zs series positively covary (i.e., C (Ws, Zs) > 0) at morphodynamically relevant water stages (Pasternack et al., 2018a). Vice versa, channel dimensions with negative Ws and Zs covariance (i.e., C (Ws, Zs) < 0) are thought to be asynchronous with flow convergence routing driven hydrodynamics and unstable in rivers at channel-altering discharges, unless the bed is highly resistant to hydraulic forcing. Many rivers have bed and bank material that resists transport for some range of low discharges and at these flows the topography exhibits negative Ws and Zs covariance. Rivers that exhibit negative Ws and Zs covariance even for very large floods tend to be extremely resistant to erosion and therefore experience morphodynamics by other mechanisms, such as knickpoint migration, potholing, chemical weathering, and freeze–thaw.

Because of its ability to discern between these two topographic regimes, the GCS of Ws and Zs has previously been utilized to predict at which stage fluvial hydraulics switch from minimally channel altering to having appreciable, channel altering flow convergence routing morphodynamics (Brown & Pasternack, 2017). GCS analysis can be used to study flow convergence routing via quantification of Ws and Zs over a range of discharges. Because GCS analysis requires only a DEM as an input (Pasternack et al., 2021), without numerical modeling or reliance on discharge-stage data, it is possible to study remote fluvial topographies that are less impacted by human alterations (Wohl, 2019). Incidentally, the same GCS has been found to be an important control on river hyporheic exchange rates (Movahedi et al., 2021), so the methodology is relevant beyond just morphodynamics.

Flow convergence routing theory dictates that it may take stronger forces than can be produced within a given channel dimension to change and control a channel at that dimension. Therefore, resilient low-flow channel dimensions may be maintained by patterns of topographic nonuniformity at higher water stages capable of making channel alterations. Most past studies have only evaluated in-channel flows and have found some sediment transport but have not observed and constrained wholesale landform re-organization at those flows (e.g., Jackson & Beschta, 1982). Theoretically, a similar relationship between bankfull and flood-stage channel dimensions could also exist but has been less studied. These concepts highlight a need to move beyond typical fluvial research where the landforms and morphodynamics of a given channel dimension are understood by considering drivers for that same dimension.

Pasternack et al. (2021) recently reported that confined mountain rivers with coarse bed material and exposed bedrock have a threshold stage at which the GCS between Ws and Zs changes from negative to positive. This provides a simple test to determine what discharge it takes to not merely move bed sediment but organize fluvial landforms via flow convergence routing. What remains unknown is the extent to which cross-sections with positive Ws and Zs values occur at different water stages across diverse river types, and whether they have riffles/pools, other riverbed units (e.g., cascades, steps, alternate bars, and lateral benches), or no units at all (e.g., a uniform canal).

3 | STUDY REGION

California's South Coast region (Figure 1) is a regulatory area defined by the California Water Board (Byrne et al., 2020) along the state's

Is flow convergence routing a likely driver of observed channel bed elevation at a given water stage?
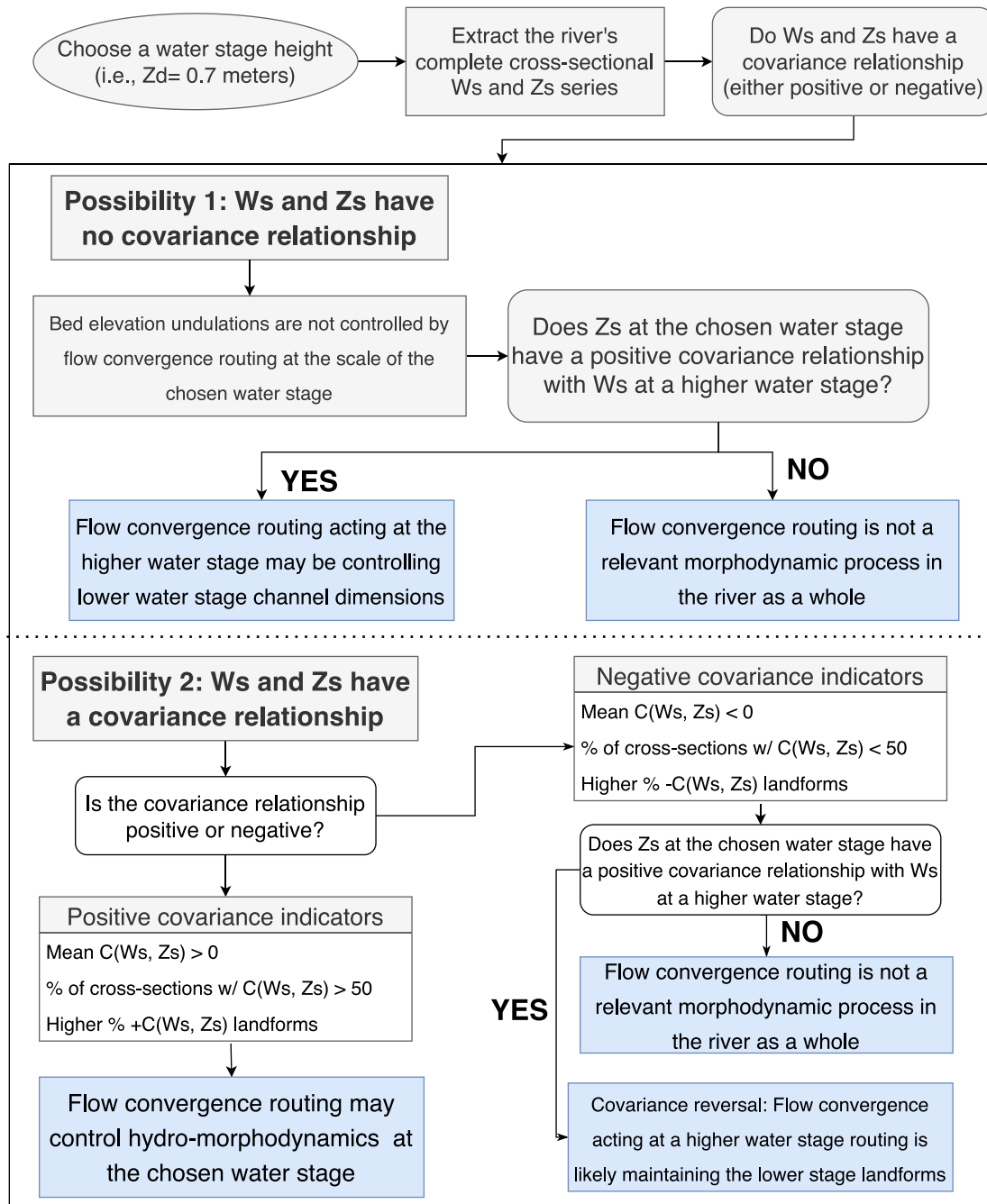
FIGURE 3 Flow chart showing different possible Ws, Zs covariance relationships, and what they indicate regarding flow convergence routing's potential role as a channel altering fluvial mechanism (shaded blue).

southern Pacific coastline. The region consists of coastal valleys, foothills, and rugged coastal mountain ranges that loosely share physiographic characteristics despite significant geologic diversity. The South Coast region has a largely dry summer subtropical climate with seasonal precipitation bipolarity (Inman & Jenkins, 1999., Abatzoglou et al., 2009). There is typically little to no precipitation from May to October followed by atmospheric river-driven precipitation during the November to April wet season (Dettinger et al., 2011; Polade et al., 2017), though even then rainfall is intermittent. Consequently, streams are typically dry for months at a time, and some are dry most

of the time. South Coast precipitation is also spatially heterogenous, made evident by the 30-year mean February precipitation, historically the wettest month of the year, ranging from 8 cm to 30.5 cm (Hill et al., 2016) within the region.

Pacific coastal U.S. rivers are generally sediment rich, and the South Coast region is no exception. Active and complex faulted geology in the mountain regions, an abundance of unconsolidated Cenozoic sediments, as well as erodible sedimentary lithologies all contribute to high rates of hillslope denudation during wet season precipitation events (Inman & Jenkins, 1999). Inter-annual ENSO-

driven climatic variability can also contribute to hillslope denudation; strong El Niño years, which reoccur roughly every five years, have resulted in 27x increases in South Coast stream sediment fluxes (Abatzoglou et al., 2009; Inman & Jenkins, 1999). In addition, the region's wildfire regime alters soil conditions (Wohlgemuth et al., 1999) and increases hillslope smoothness (Roth et al., 2020). When wildfires are followed by intense wet season rainstorms, then mass wasting loads rivers with large quantities of sediment (Warrick et al., 2012).

Byrne et al. (2020) and Lane et al. (2021) published a South Coast regional river classification with five river types (Table 1; Figure S1) based on a rigorous, equal-effort, three-way (valley confinement, sediment supply, and local slope versus contribution area bin) stratified random sampling strategy (n = 67 measured reaches). A river type was defined as an archetypical stream form at the 10–20 channel width scale (e.g., riffle-pool, plane bed) that has well-defined: (a) channel attributes (e.g., slope, bankfull width), (b) topographic variability attributes (e.g., coefficients of variation of width and depth), (c) sediment composition and (d) valley widths. Classification methodology details can be found in the Supplementary Material file.

Guillon et al. (2020) developed a Random Forest machine learning algorithm that predicts river type for any 200-m river interval along National Hydrography Dataset version 2 streamlines (McKay et al., 2012; NHDPlusV2) in any California region. Byrne et al. (2020) further expanded and improved the algorithm and then applied it to all California coastal regions, including the South Coast region. The final, best Random Forest model for the South Coast (cross-validated multiclass area under the receiver operating characteristic curve of 0.949; cross-validated accuracy of 82.1%) was trained on the river type labels for 67 observed reaches and used 147 potential predictors quantifying metrics of river corridor terrain, river network topology, topographic fractal dimension, sediment supply, valley confinement, and contributing drainage area. This yielded a population of South Coast 200-m stream intervals with expected river types to draw from for use in a mindful, equal-effort sampling campaign in our experimental design.

Based on the field data and machine learning predictions, South Coast river types have an unequal abundance in the region, and each type has representative geomorphic attributes (Table 2; Figure 4). The most abundant type is type 5 (partly confined, gravel-cobble, riffle-pool), while types 2 (partly confined gravel, braided) and 3 (confined, bounder, cascade/step-pool) are present in almost equal low abundance. All river types have relatively small catchment area <200 km^2.

TABLE 1 South Coast geomorphic river type descriptions (Byrne et al., 2020), and their respective sample sizes.

River type	Description	# of river reaches (N)
1	Unconfined, uniform, sand-gravel	6
2	Partly confined, high W/D ratio, split-channel	6
3	Confined, cobble-boulder, cascade/step-pool	7
4	Confined, uniform, gravel-cobble	8
5	Partly confined, riffle-pool, gravel-cobble	8

4 | METHODS

To answer the scientific question in detail for sufficient river reaches to obtain a regional synthesis, this study had to advance geomorphic analysis methods through development of a new algorithm and then apply that within a rigorous experimental design to test specific alternative hypotheses. The approach involved producing, analyzing, and comparing many meter-scale fluvial DEMs to reveal and characterize similarities and differences in topographic patterning explained by flow convergence routing's relative importance as a channel altering mechanism in ephemeral rivers. With that scope in mind, this section presents the study-specific information and data used to obtain the results and test hypotheses without describing or justifying all aspects of GCS theory and methods addressed in previous publications.

4.1 | GCS analysis software

Until now, GCS analysis has been performed manually using ArcGIS® and Microsoft Excel® (Pasternack et al., 2018b, 2021), which limits the number of reaches that can be analyzed and raises the potential for manual error at many steps without mindful quality control. This study introduces a free, open source Python3 program (https://github.com/xaviernogueira/gcs_gui) that reproduces and semi-automates the existing GCS workflow (Figure 5) while adding several new outputs and analyses, including ones that synthesize results at larger spatial scales. A detailed user's manual is published at https://gcs-gui-documentation.readthedocs.io/.

The program requires a topo-bathymetric LiDAR point cloud LAS file as the primary input. Expert-based user input then specifies three things: (i) LiDAR processing parameter values used in LasTools, (ii) thalweg elevation profile breakpoints in support of bed-elevation detrending (fourth subsection of this section) and (ii) a set of key water stage values above Zd (hereafter, Zd stages) that are representative of geomorphically, hydrologically, or ecologically significant inundation levels (fifth subsection of this section). The program requires LasTools (Hug et al., 2004), ESRI ArcPro's Python3 package "arcpy" (with a valid "spatial analyst" license), and a few free Python packages (i.e., pillow, plotly, seaborn, and openpyx1).

As the main feature, the program automates production of downstream spatial series of Ws, Zs, C (Ws, Zs), and flow convergence routing landform code values for all selected key Zd stages. It also produces a set of reach-average river metrics by Zd stage that can be used for river classification. From the primary GCS spatial series, the program then carries out several analyses to evaluate GCS patterns and flow convergence routing conditions. Analyses include data tables of indicator metrics and plots of results.

4.2 | Experimental design

Given the new GCS program, a mindful experimental design was needed to answer the study questions by analyzing GCS outputs to compare and contrast results among many reaches and their three characteristic water stages. The first step involved developing a river-reach sampling scheme (third subsection of this section). Even though

TABLE 2 Median channel attributes[a] of South Coast channel types from Byrne et al. (2020) and % of regional stream length[b] for each type.

	%		km²				(m)			(mm)	
Type	Of length	s	Ac	w/d	CVd	CVw	C	d	w	D50	D84
1	15	0.0053	52	10.0	0.24	0.20	2,480	0.63	6.67	5.6	22.6
2	11	0.0143	124	36.7	0.25	0.30	202	0.42	17.92	10.8	48
3	10	0.0397	28	9.7	0.32	0.28	31	0.54	4.94	90	2000
4	20	0.0182	25	9.6	0.21	0.21	94	0.64	5.68	11	190
5	44	0.0054	182	12.8	0.35	0.28	126	0.60	7.78	16	128

[a]Contributing area (Ac), bed slope (s), bankfull depth (d) and width (w), coefficient of variation (CV), median (D50 and 84th percent (D84) of grain size, valley confinement (C).
[b]Sum of 200-m stream intervals for each river type throughout the stream network of the region, with type designations predicted using a Random Forest machine learning algorithm (Guillon et al., 2020).
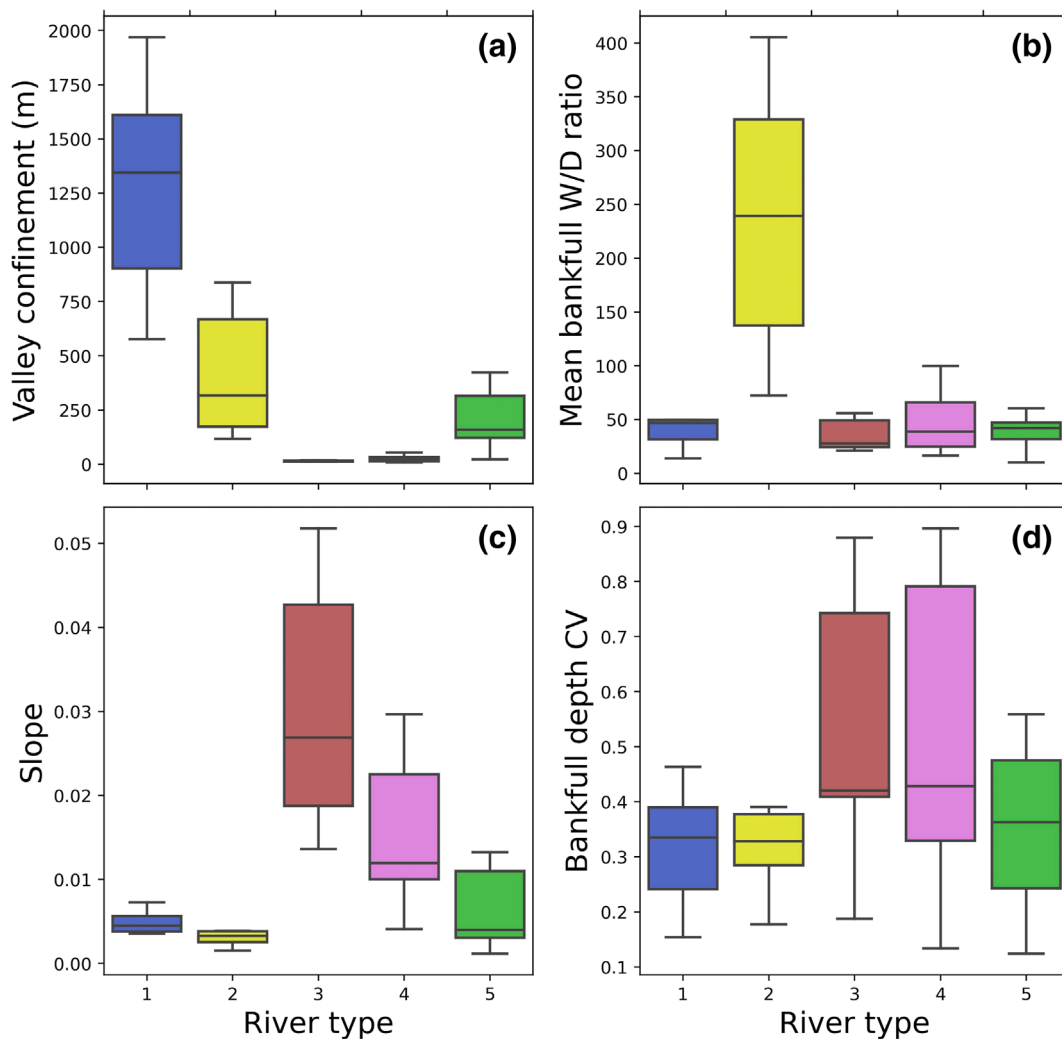
FIGURE 4 Distribution of valley confinement distance (A), bankfull width to depth ratio B), slope (C), and bankfull depth coefficient of variation (D) values for 5–8 study reaches per river type (35 reaches total). See Table 1 for river type descriptions.

GCS analysis is now reasonably automated, in this first regional-scale implementation we did not aim to extract and analyze entire river networks, as some expert decisions and quality checks must be made for every study reach. The initial expectation of river type came from the pre-existing river type predictions for the South Coast region (Byrne et al., 2020).

Once selected, individual reaches were put through the GCS program to obtain standard GCS analysis outputs and reach-average river classification metrics based on airborne LiDAR data. Next, program outputs were used to verify and possibly update river types (seventh subsection of this section). Finally, Python scripted analyses were used to produce statistics, plots, and tables that tested the hypotheses

and through such tests addressed the specific scientific questions providing insight about the broad scientific question (Figure 2).

4.3 | River type sampling

To reduce possible bias and avoid noticeable geographic patterning in the analysis related to river reach sample quantities, relatively even numbers of samples of each river type were assembled. The population of 200-m river intervals from Byrne et al. (2020) was clipped to be within the area of available, suitable dry-season LiDAR data producing full river-corridor topography (i.e. no standing water that near-infrared airborne LiDAR could not penetrate). Among those intervals, the population was further reduced to isolate reaches with ephemeral hydrology, as identified by a statewide hydrologic classification's "Flashy-Ephemeral River" designation (Lane et al., 2018).

From the population of all ephemeral reaches with LiDAR coverage and machine-learning predicted river types, eight were randomly selected for each river type. These forty (8 × 5) sites served as a

representative initial sample set to undertake further characterization to determine final suitability for use in the study. The sites were not yet considered final, because the study's analysis of dense LiDAR point clouds yielded classification metrics that could check the machine learning river-type prediction and possibly override it (seventh subsection of this section) for a more accurate classification beneficial for this study.

4.4 | DEM generation, clipping, and detrending

Meter-resolution, bare ground raster DEMs were generated in our software for a long, wide interval of fully dry river-corridor terrain. Figure 5a summarizes the methodology, with full details provided in the Supplementary Material file along with data tables and a set of detrended DEMs for every study site (also reporting their key reach metrics). DEMs were closely examined for quality issues. For example, reaches with water-filled pools or artificial human confinements (levees, walls, etc.) were removed from the sample set reducing the original 40 reaches down to 35.
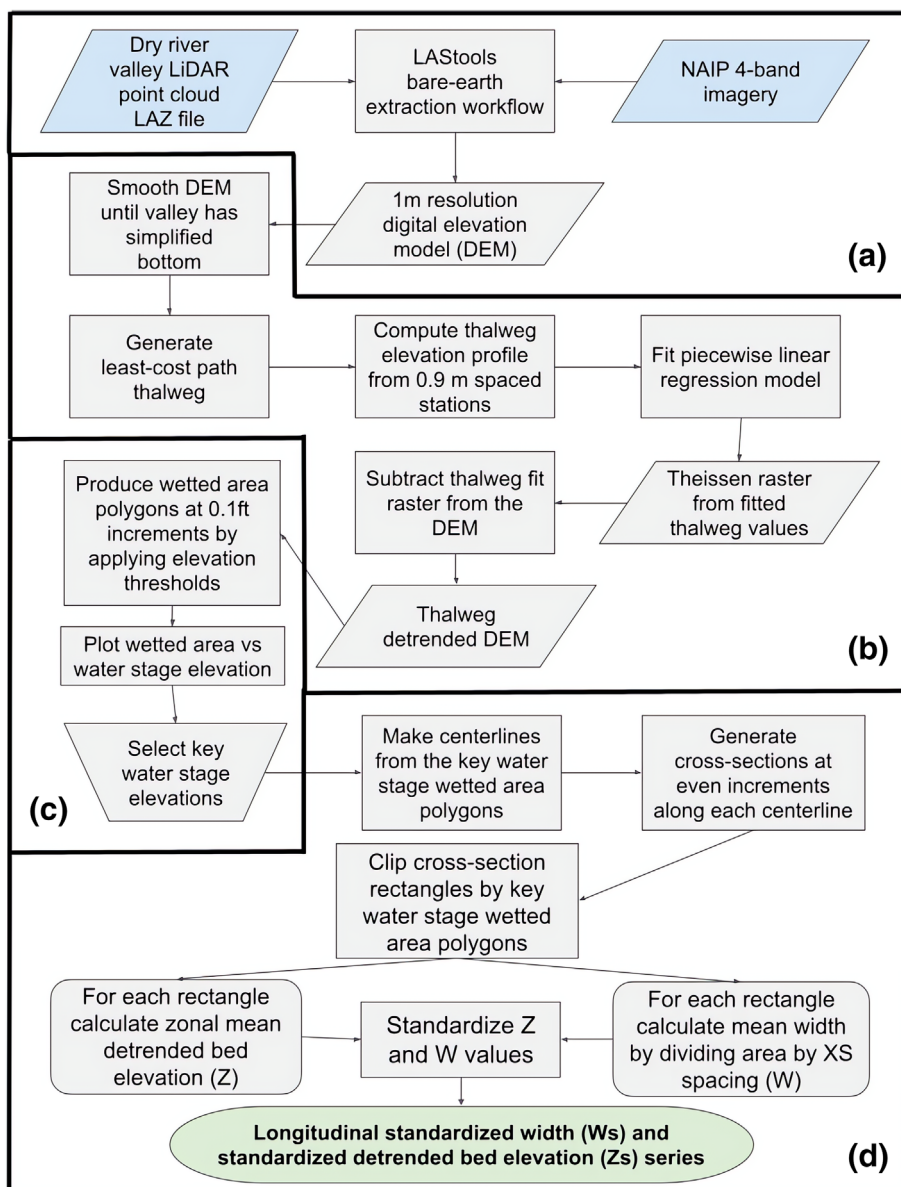

FIGURE 5 Flow chart showing the LiDAR data processing methodology that outputs baseflow, bankfull, and flood-stage longitudinal standardized width (Ws) and standardized, detrended bed elevation (Zs) series.
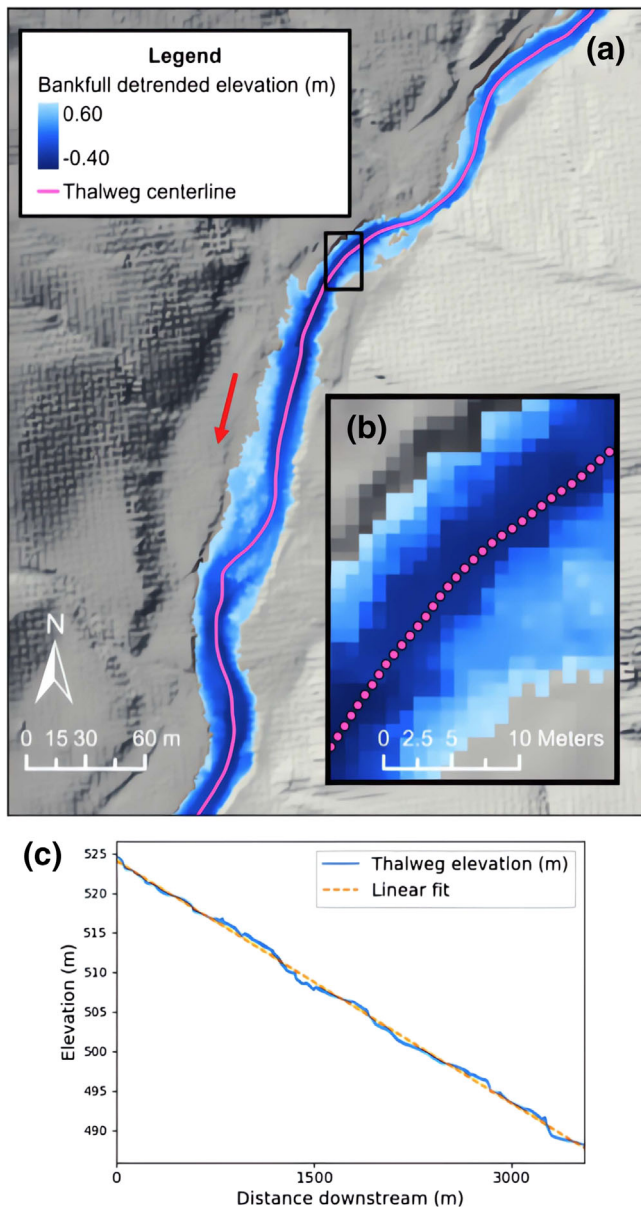
FIGURE 6 Detrended DEM of site 17585756 clipped to the bankfull wetted area, overlaid on a non-detrended hill shade DEM (A), of a partly confined, riffle-pool reach (river type 5). Shown as well are the 0.3 m spaced thalweg elevation sampling points (B), as well the corresponding longitudinal elevation profile and its linear regression fit (C).

Each DEM's length was clipped to yield a persistent geomorphic reach of a single river type. After the whole workflow was performed and mean bankfull channel width was computed, it was possible to determine that average reach length was 56 times that width. These spans are sufficiently long for GCS analysis and are consistent with classic reach length norms (>10–20 times bankfull width) for reach-scale studies.

GCS analysis focuses on local fluvial topographic variability as a hydro-morphodynamic driver via topographic steering. Local variability is evidenced in longitudinally detrended DEMs (e.g., Figure 6). DEM detrending of each reach was performed using the steps in Figure 5b (details in the Supplementary Material file, which includes maps of all detrended DEMs).

4.5 | Baseflow, bankfull, and flood Zd stage designation

To compare fluvial topography among river reaches and river types this study followed Pasternack et al. (2021) to define "Zd stages", which are horizontal water surface elevation (Zd) planes above the detrended bed elevation. A Zd stage is similar to the "height above nearest drainage" from the hydrology literature (Nobre et al., 2011), except Zd stage has a single detrended vertical datum for a reach, not a locally relative datum based on the nearest stream line. Also, this study used 1-m DEMs, not 10 or 30 m DEMs, typically of hydrological studies. This method has been extensively evaluated and corroborated (e.g., Annis et al., 2019; Hocini et al., 2020; Rathjens et al., 2016).

Next, objective analyses aided identification of geomorphically significant inundation areas that are present among all sites, even though sampled rivers came in different shapes and sizes. Similar identification approaches are rapidly proliferating (e.g., David et al., 2017; Lindroth et al., 2020; Wheaton et al., 2013; Zheng et al., 2018), with specific justification of this approach in the Supplementary Materials file. For each sampled river, a Zd stage is designated that corresponds to a longitudinally persistent, eco-geomorphically relevant stage threshold; at a minimum, stages corresponding to "base flow" and "bankfull" discharges are used (Figure S1 in the Supplementary Material file). Unless the floodplain is exceptionally flat and wide, one or more flood stages should be included, such as each stage associated with different macro-channel bench tops (Erskine & Livingstone, 1999), the stage inundating the flood prone area (Pasternack et al., 2021), and/or the stage filling the alluvial valley floor. The more Zd stages analyzed, the more complex the analysis and interpretation of how all the stages work together, which remains an open challenge for future GCS development.

Zd stage selection is an expert-based process facilitated by an analysis of lateral slope breaks across a river corridor's width and inspection of aerial imagery (Figure 5c). Methodological details are provided in the Supplementary Material file. The South Coast's ephemeral rivers do not have perennial, groundwater-derived "base flow" (Dettinger et al., 2011; Polade et al., 2017), but they do tend to have a flat channel bottom, sometimes containing many large bed elements. For this study, baseflow Zd stage was defined as that just fully inundating the relatively flat riverbed along the majority of the thalweg's longitudinal extent. DEM detrending results in high riffle crests protruding above the baseflow Zd stage because topographic analysis cannot account for hydraulic backwatering (Pasternack et al., 2021).

In addition to a baseflow Zs stage, this study used bankfull Zd stage and one flood Zs stage. Stage indicators for geomorphically significant flows often differ between channel types because unconfined alluvial rivers can have extensive flat floodplains, while confined bedrock rivers rarely do. In partly confined and unconfined valleys, bankfull Zd stage was defined as that inundating a geometrically well-defined channel bounded by a comparatively flat depositional surface (i.e., floodplain). In confined canyons without floodplains, bankfull Zd stage was delineated to exclude densely vegetated peripheral areas lacking non-boulder, active, alluvial bed sediment. Figure 6 and the full set of reach DEMs in the Supplementary Material file portray the bankfull Zd stage in shades of blue.

In partly confined valleys, flood Zd stage was defined as the lowest stage inundating the alluvial valley and contacting confining valley walls. In some unconfined settings with especially distal valley walls, a flood Zd stage may be defined regarding a prominent terrace feature that limits the wetted areas corresponding to all realistic water stages. Flood Zd stage can be defined similarly in some confined settings as well, in which a small but observable alluvial valley is present. In the most tightly confined reaches without any semblance of a floodplain, flood Zd stage is defined by both the slope break above which wetted area accumulation increases linearly with Zd stage and careful visual interpretation of paleo-flow indicators.

4.6 | GCS data extraction

GCS analysis requires Ws and Zs data from evenly spaced cross-sectional rectangles along the river corridor (Figure 3). To account for a river's flow path changing with discharge a unique centerline was generated for each Zd stage in each reach by bisecting the stage's wetted area polygon. Cross-sectional rectangles (hereafter "rectangles") were generated and stationed at ∼1/20th of bankfull width (but larger than the dimensions of a single raster pixel). Mean wetted width (W), Ws, mean bed elevation (Z), Zd, and Zs were computed for each rectangle. Geomorphic covariance, C (Ws, Zs), was calculated using the product (Ws·Zs) to obtain a spatial series at each key Zd stage (Figure 7). A decision tree (Figure S4) was used to classify each rectangle into one of five stage-independent, morphodynamics-specific landform types: "normal channel" (Ws and Zs values −0.5-0.5), "nozzle" (Ws < −0.5, Zs > 0.5), "wide-bar" (Ws and Zs > 0.5), "constricted pool" (Ws and Zs < −0.5), or "oversized" (Ws > 0.5, Zs < −0.5) (Pasternack et al., 2018b).

4.7 | River type verification

The 35 study sites obtained through the sampling procedure had an initial river type predicted with the Random Forest machine learning model. Uncertainty in those predictions arises from both the classification and prediction steps (Byrne et al., 2020). To increase the accuracy of river type designation for this study, within the limitations of classification itself as a paradigm, four reach-average channel attributes driving South Coast river type classification (Byrne et al., 2020) provided a quantitative basis for verifying and, if needed, updating classification: slope, valley confinement distance, bankfull width to depth ratio, and bankfull depth coefficient of variation (Figure 4). The GCS program was used to compute these variables at bankfull Zd stage for each site's DEM. Resulting values were used in the existing classification and regression tree for determining South Coast river types at each site (Byrne et al., 2020), with the exception that no grain size classification metrics were available.

After verification and some re-assignment, each river type had six to eight samples (Table 1). Sensitivity analysis was conducted to assess the extent to which river type sample sizes impacted type-averaged GCS metrics. Group sample sizes were sufficient to prevent a single river reach from significantly affecting type-averaged GCS values. Detailed characterizations of each site are in the Supplementary Material file.

4.8 | Data analysis

For question O1a, if channel width and bed elevation are independent, then the expectations for mean C (Ws, Zs) and % of C (Ws, Zs) values >0 are 0 and 50%, respectively. Results significantly above or
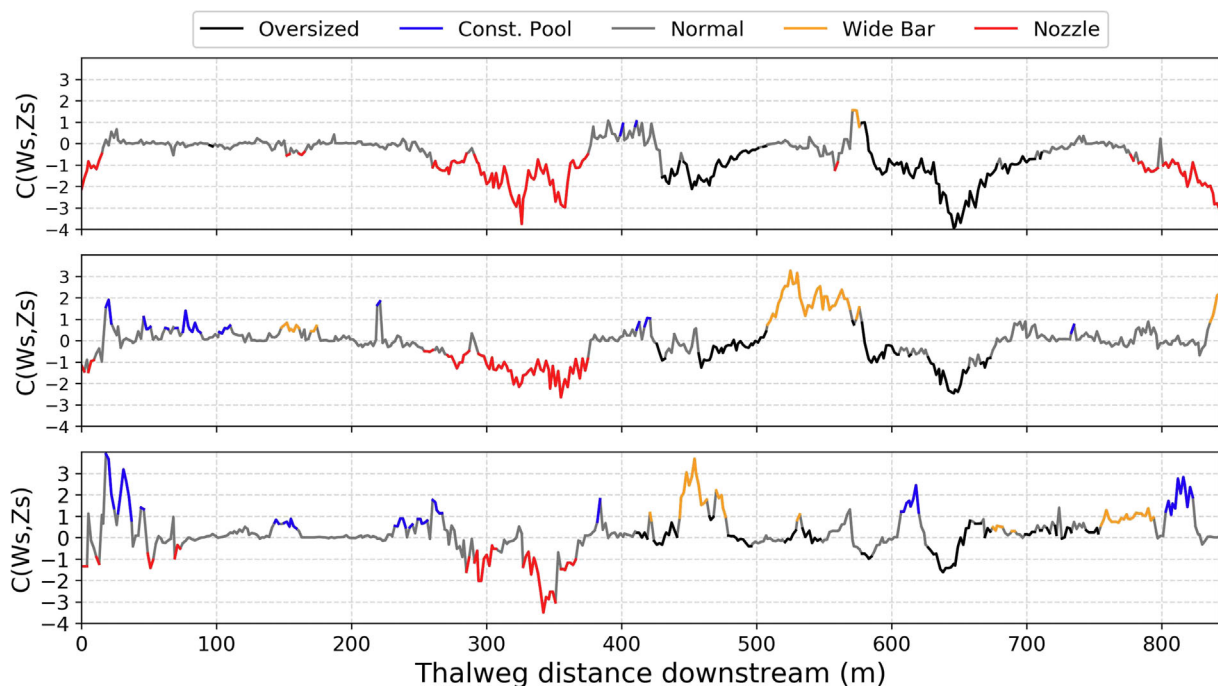

FIGURE 7 An example of C (Ws, Zs) series from site 17585756 at baseflow (A), bankfull (B), and flood-stage (C). Positive values represent rectangles where Ws and Zs have the same sign, while negative values occur when they have opposite signs. Landform designations are color coded (CP is blue, WB is orange, NZ is red, O is black, and NC is gray).

below expectation indicate the Ws and Zs are co-varying to yield a coherent pattern per hypotheses. To address question O1a, values for each metric were grouped among all rivers for their whole lengths by river type at each Zd stage. With two metrics, five river types, and three stages, this yielded 30 datasets to test against the indicator values.

In addition, the non-parametric Mann–Whitney U test (aka Wilcoxon rank-sum test) was employed to directly compare whether two independent samples come from the same population or have the same distribution (Mann & Whitney, 1947). This test does not require data to be normally distributed and accepts samples with unequal counts. The assumptions of this method were met for this data. A sample is the set of all values of a covariance metric, C (Ws, Zs) or % of C (Ws, Zs) values > 0, aggregated among all reaches in a given river type at a single Zd stage. Such aggregation yielded large point counts for each sample.

In this study, the Mann–Whitney U test was run two ways. In the first usage, the comparison was between Zd stages for a given river type. This test provides statistical confidence ($p < 0.05$) as to whether each covariance metric is really shifting significantly as stage increases. Such a shift would be expected if there is a transition from negative to positive covariance indicating the onset of flow convergence routing and if there is increasing strength of flow convergence routing after that transition. In the second usage, the same metrics and samples were tested, but this time comparing between river types at a given stage. This test provides statistical confidence ($p < 0.05$) as to whether flow convergence routing is active and stronger for one river type compared to another at a given stage.

For question O1b, all paired Ws and Zs rectangle values from our full sample were grouped first by river type, and then by key Zd stage (five types times three stages yielded 30 subsets). For each two-way stratified dataset, a density heat plot was produced that visualizes the distribution of all rectangle geometries as captured their standardized Ws and Zs values. Because of the nature of standardized values, a symmetrical, Gaussian-like joint distribution would affirm the null hypothesis that width and bed elevation have no structured relationship. Because thousands of rectangles are visualized in each heat plot, any noticeable non-Gaussian-like skews or linearity are unlikely to emerge by chance. To address hypotheses, heat plots were qualitatively compared and interpreted across the key water stages for each river type, as well as across river types at the analogous Zd stages.

For question O1c, the relative abundance of rectangles with each landform classification at baseflow, bankfull, and flood Zd stage was calculated for each study reach (i.e., % nozzle, % wide bar, etc., among all rectangles in a reach for each Zd stage). Next, we consolidated these relative abundance values first by river type, and then sorted them by key Zd stage. In lieu of a relationship between Ws and Zs for a river type at a given Zd stage, we would expect to see approximately uniform abundances of the different landforms (excluding normal), so this was tested first. The analysis of variance test (ANOVA) produces p values representing the probability that observed discrepancies between averaged landform relative abundances are statistically significant. Additionally, separate hypotheses predicted that certain landforms will be differently abundant across river types at the same Zd stage. We addressed these with a different ANOVA that compared the average abundance of each landform type (excluding normal) across river types to a uniform distribution. Hypotheses were

considered corroborated only if the observed landform abundances matched predictions and were significantly differ from a uniform distribution, as indicated by an ANOVA p value < 0.05.

For question O2a, for each river type, we identified the subsets of rectangles with high Zs (> 0.5) and low Zs (< −0.5) at baseflow and bankfull Zd stages. We then extracted the Ws values of these rectangles at the next higher Zd stage, either bankfull or flood. To address hypotheses, we paired and compared the distributions of the higher Zd stage Ws values associated with high and low bed elevation. To do so we visualized each pair of Ws distributions in Violin plots and used a Welch's t-test (Yuen, 1974) to test whether population averages were significantly different at the 95% level ($p < 0.05$). Welch's t-test assumes that input datasets are sampled from populations that follow a normal distribution. Because Ws values are normalized, these datasets meet the assumption.

For question O2b, for both baseflow-in-bankfull and bankfull-in-flood landform nesting, we identified all rectangles that changed from one flow convergence routing landform to another (excluding normal). To address hypotheses, we assessed for each river type whether any specific landform nesting was over or underrepresented relative to random change using Chi-Square tests (Lowry, 2017). The tests checked the significance of discrepancies between the expected and observed frequency of each unique landform nesting. The Chi-Square test's "expected frequency" parameter was set to the relative abundance of landforms at the higher paired water stage. This allowed preferred nesting structures to be tested for significance relative to any changes in landform abundances between water stages. For example, if on average 15% of a river type's flood stage rectangles are classified as wide bars, then the expected frequency for any bankfull landform nesting in wide bar is 15% as a null hypothesis. Much higher values and a significant test result would then indicate a preferential landform nesting pattern.

Sankey plots were produced to visually represent nesting results. In these plots, each column presents results for a different water stage (increasing from left to right) and depicts the relative abundance of each landform type (excluding normal) as the height of a colored bar. Further, the relative abundance of nesting of a lower stage's landforms (to the left) within each of a higher stage's landforms (to the right) is depicted with the thickness of gray pathways connecting nested landforms.

5 | RESULTS

All outcomes of question-specific hypothesis tests are color coded in accordance with our study findings in Figure 2 to provide a simple, fast summary of the entire study's findings.

O1a. Are there low and high Ws·Zs covariance values for baseflow and bankfull stages, respectively?

Results corroborated the hypothesis that both covariance metric values, mean C (Ws, Zs) and % C (Ws, Zs), would be lowest (more negative Ws, Zs covariance) for all river types at baseflow, and then increase with stage (Table 3). Shifting from baseflow to bankfull stage,

TABLE 3 Question O1a. Mean covariance metrics for river reaches within each river type calculated at each flow-stage. Metrics are as follows; mean rectangle covariance (top), and percent of rectangles with positive C (Ws, Zs) values (bottom).

	Mean C (Ws, Zs)					
	Baseflow		**Bankfull**		**Flood stage**	
River type	*Mean*	*STD*	*Mean*	*STD*	*Mean*	*STD*
1	−0.09	0.28	0.38	0.22	0.09	0.22
2	−0.07	0.18	0.27	0.47	0.29	0.30
3	−0.52	0.17	−0.02	0.30	0.29	0.16
4	−0.39	0.24	0.10	0.38	0.22	0.34
5	−0.35	0.14	0.28	0.28	0.22	0.35
	% C (Ws, Zs) > 0					
	Baseflow		**Bankfull**		**Flood stage**	
River type	*Mean*	*STD*	*Mean*	*STD*	*Mean*	*STD*
1	47.6	12.2	61.5	12.7	59.4	9.8
2	48.9	7.6	59.6	19.3	60.3	11.4
3	29.7	7.2	50.6	9.8	60.7	6.4
4	33.7	11.2	53.5	15.1	57.2	15.3
5	38.3	7.4	58.6	10.3	53.1	19.7

TABLE 4 Mann–Whitney U test results comparing Zd stages. Gray shading indicates results with $p < 0.05$.

(A) Mean C (Ws,Zs)

	River type				
Stage transition	1	2	3	4	5
base-bank	0.026	0.180	0.004	0.005	0.000
bank-flood	0.052	0.937	0.053	0.645	0.959
base-flood	0.429	0.065	0.001	0.002	0.007

(B) % C (Ws,Zs) > 0

	River type				
Stage transition	1	2	3	4	5
base-bank	0.065	0.589	0.002	0.005	0.000
bank-flood	0.662	1.000	0.038	0.574	0.959
base-flood	0.177	0.093	0.001	0.002	0.065

TABLE 5 Mann–Whitney U test results comparing river types. Gray shading indicates results with $p < 0.05$.

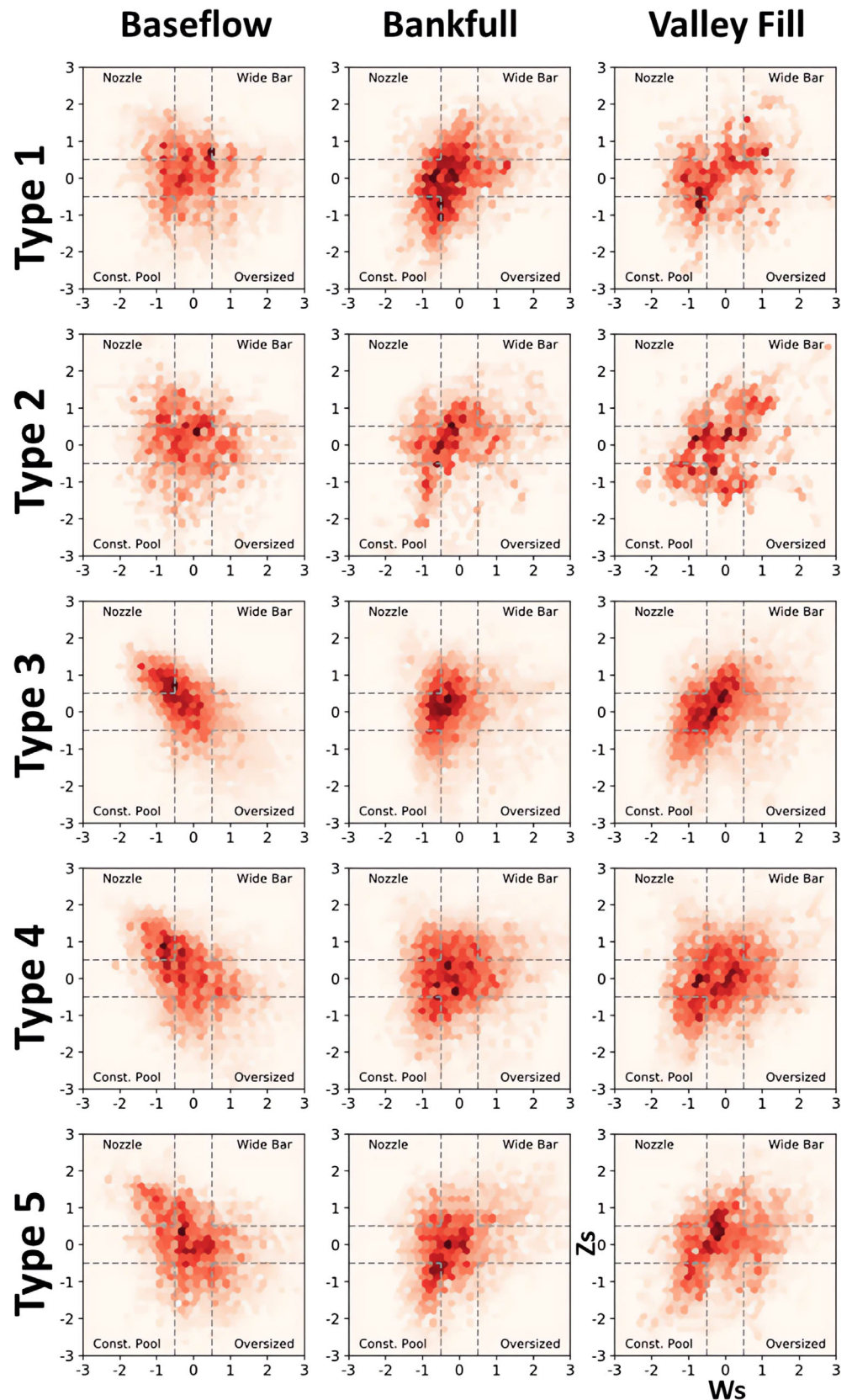| | **p-Values** | | | |
(A) Baseflow mean C (Ws,Zs)				
	1	2	3	4
1				
2	0.699			
3	0.008	0.005		
4	0.029	0.029	0.189	
5	0.228	0.008	0.094	0.328
(B) Bankfull mean C (Ws,Zs)				
	1	2	3	4
1				
2	0.937			
3	0.035	0.295		
4	0.108	0.414	0.336	
5	0.282	0.852	0.094	0.574
(C) Flood mean C (Ws,Zs)				
	1	2	3	4
1				
2	0.177			
3	0.106	0.731		
4	0.724	0.491	0.779	
5	0.222	0.755	0.694	0.878
(D) Baseflow % C (Ws,Zs) > 0				
	1	2	3	4
1				
2	0.589			
3	0.008	0.005		
4	0.02	0.02	0.336	
5	0.345	0.043	0.072	0.161
(E) Bankfull % C (Ws,Zs) > 0				
	1	2	3	4
1				
2	0.818			
3	0.073	0.445		
4	0.345	0.573	0.694	
5	0.573	1	0.189	0.382
(F) Flood % C (Ws,Zs) > 0				
	1	2	3	4
1				
2	1			
3	0.755	0.731		
4	0.833	0.755	0.536	
5	0.724	0.755	0.463	0.878

both metrics increased for all river types, though type 2 (split channels) increased the least and had the largest standard deviation at bankfull Zd stage (Table 3). River types 3, 4, and 5 each had on average ~20% more positively covarying rectangles at bankfull than at baseflow. At bankfull, all river types had on average >50% of rectangles with positive C (Ws, Zs) values. Additionally, all river types had mildly positive mean C (Ws, Zs) except for river type 3, which makes sense given that it is a confined type. The Mann–Whitney U test found that these shifts from baseflow to bankfull stage were statistically significant for all river types except type 2 for mean C (Ws, Zs) and for types 3–5 for % C (Ws, Zs) > 0 (Table 4). Type 2 has such diverse configurations, including both anastomosing and braided examples, that its internal variation appears to mask differences in flow convergence routing, with some subtypes having it strongly and others not.

Comparing bankfull and flood stages, both mean C (Ws, Zs) and % C (Ws, Zs) > 0 did not significantly differ between stages in river types 1, 2, 4, and 5. River type 3 experienced a statistically significant 0.30 increase in mean C (Ws, Zs) going from bankfull to flood stage, as well as a ~10% increase in positively covarying rectangles on average ($p = 0.045$ and $p = 0.046$ respectively). All Mann–Whitney U tests

FIGURE 8 Question O1b. Heat plots showing 2-D distributions of paired rectangle Ws (x-axis) and Zs (y-axis) values. Flow convergence routing landform thresholds are displayed with dashed lines. Plots in the same column show analyses at the indicated water stage. Plots in the same row show analyses for the indicated river type. See Table 1 for river type descriptions.

also found that differences in metrics between these stages were statistically insignificant, except for type 3, for which the p-values were 0.053 and 0.038 for mean C (Ws, Zs) and % C (Ws, Zs) > 0, respectively.

Results do not support either of our river-type-specific hypotheses but show some differences between types consistent with expectations (Tables 3, 5). While river type 1 had the highest average covariance metric values at bankfull, they were not statistically significantly higher than flood stage as predicted. Additionally, river type 2 did not have the lowest average covariance metric values of all river types at any water stage. Mann–Whitney U test results showed statistically different baseflow stage covariance metrics separating unconfined river types from confined and partially confined types. Confined and partially confined types were not differentiated at that

stage. At higher stages, types are not statistically differentiated, because they all exhibit the indicators for flow convergence routing (Table 5).

O1b. Do stage-dependent joint distributions of rectangle Ws and Zs values display non-Gaussian organization, and does this vary by water stage or river type class?

Results vary by valley confinement. River type 1 (unconfined, uniform, sand/gravel) joint Ws, Zs distributions have a roughly Gaussian form at both baseflow and flood stage (Figure 8). At bankfull the distribution is noticeably skewed towards positive C (Ws, Zs) (i.e., positive sloping linearity), which supports the hypothesis.

In partly confined ephemeral rivers, the character of Ws-Zs distributions is different between the two river types (Figure 8). River type 2 (partly confined, high W/D ratio, split-channel) has roughly Gaussian Ws-Zs distributions at baseflow. In contrast, river type 5 (partly confined, gravel/cobble, riffle-pool) has a baseflow distribution with a notable tear-drop-shaped skew towards negative covariance. Both river type 2 and 5 have bankfull and flood stage Ws-Zs distributions that are notably less organized, but subtly skewed towards positive covariance at flood stage. The observed flood stage skew leads us to reject our hypothesis that river type 2 will have unorganized Ws-Zs heat plots at all water stages.

In confined valleys, river types 3 and 4 have tightly clustered Ws-Zs distributions with similar skews at each water stage (Figure 8). For both river types, the bivariate distributions skew strongly towards negative Ws-Zs covariance at baseflow, show little to no directional skew at bankfull, and skew towards positive Ws-Zs covariance at flood stage albeit more mildly in river type 4. Results support the hypothesis that in confined valley settings the structure of fluvial topography is highly flow-stage dependent and more tightly organized, potentially due to valley walls limiting width variability. This was particularly evident at baseflow, where high bed elevation co-occurs frequently with relative width constrictions in a linear like fashion.

O1c. How do the relative abundances of flow convergence routing landforms vary across stages and river types?

In accordance with our hypothesis, average landform relative abundances were found to be significantly non-uniform at baseflow for river types 3, 4, and 5 (ANOVA $p < 0.05$). In each case nozzle and oversized rectangles (−Ws-Zs covariance) were more prevalent than constricted pool and wide bars rectangles (+Ws-Zs covariance). However, we also predicted that river types 1 and 2 would similarly exhibit negative covariance landforms at baseflow, which was visually observable (Figure 9) but not statistically significant. At bankfull stage, only the valley confined river types 3 and 4 had statistically significant non-uniform landform relative abundances ($p < 0.05$ level). For both types, negative covariance landforms were still more prevalent, albeit by lesser margins than at baseflow. At flood stage, river types 2 and

3 had statistically significant non-uniform relative landform abundances ($p < 0.05$), characterized for both by a scarcity of nozzles and a higher abundance of wide bars and constricted pools.

The ANOVA test applied to compare landform relative abundances between river types found significant variability in only two cases. Baseflow wide bars are significantly more common in river types 1 and 2 (mean = 9.3%). Bankfull nozzles are significantly more common in both confined river types 3 and 4. The prediction that positive covariance landforms would be significantly more abundant for river type 5 was not supported by results. However, the prediction that negative covariance landforms would be more abundant in confined river types at non-baseflow stages than other river types was found to be somewhat true at least for bankfull nozzles.

Finally, in all river types, the relative abundance of oversized rectangles (+Ws, −Zs) remained relatively constant across water stages. In river types 1, 2, and 5 the flow-stage variability of all other landform relative abundances (excluding normal) was not significant at the $p < 0.05$ level. In confined river types 3 and 4, the non-oversized, landforms vary in abundance significantly ($p < 0.05$) across water stages. In both river types, the relative abundance of wide bars and constricted pools (+Ws-Zs covariance) increases with flow-stage, contrasted to nozzles which half in abundance across both baseflow to bankfull, and bankfull to flood-stage nesting (Figure 9).

O2a. Are relative topographic highs and lows at baseflow and bankfull associated with width undulations occurring at bankfull and flood stage topography respectively?

In river types 1, 2, 4, and 5 rectangles with high bed elevation (Zs > 0.5) at baseflow had significantly greater mean widths at bankfull than rectangles with low bed elevation (Zs < −0.5) at baseflow ($p < 0.05$). This trend was particularly pronounced for unconfined river type 1 that had a mean bankfull Ws associated with baseflow topographic highs that was 0.69 standard deviations greater than the topographic lows (Figure 10). In contrast, river type 3 rectangles with Zs > 0.5 have a mean Ws value that is 0.18 lower than rectangles with Zs < −0.5. This analysis largely supported the prediction that baseflow topographic highs would be associated with higher bankfull width than baseflow topographic lows, however river type 3 was the exception.

In all river types except type 2, rectangles with high bed elevation at bankfull had a mean flood-stage Ws that was significantly greater than rectangles with low bed elevation at bankfull stage, again with river type 1 having the largest discrepancy. River type 2 mean Ws values at flood stage did not differ at the $p < 0.05$ significance level. The hypotheses that bankfull-to-flood stage preferential nesting would be observed exclusively in the more non-uniform river types 3 and 5 was not supported.

O2b. Do flow convergence routing landforms have preferred nesting structures (i.e., baseflow nozzles within bankfull wide bars)?

FIGURE 9 Pie charts addressing Question O1c by showing average relative landform abundance for each river type (rows) across key flow stages (columns).
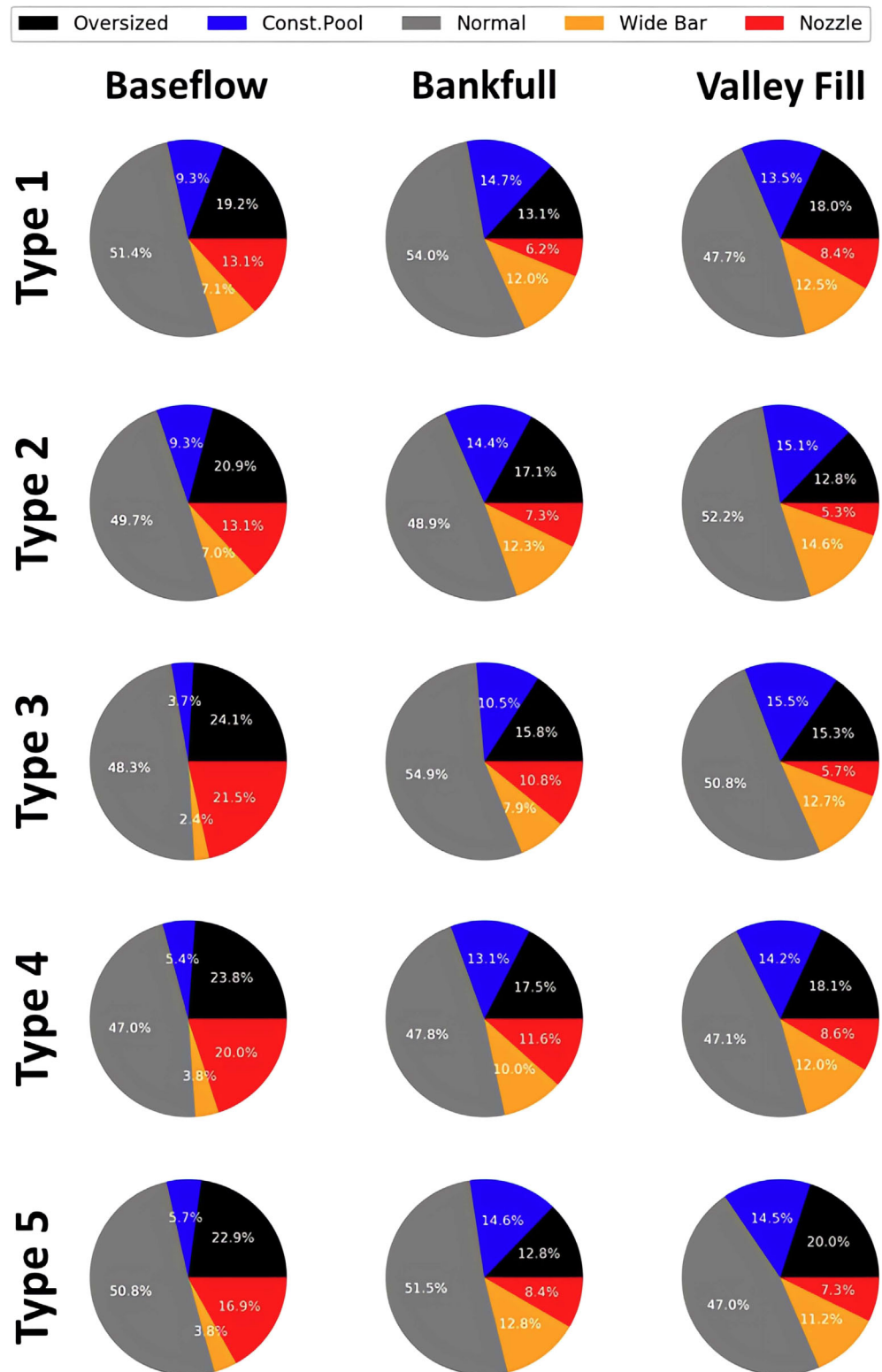
Results indicated that preferential flow convergence routing landform nesting structures exist and can be meaningfully interpreted. Significance levels for all Chi-Squared tests were exceedingly high. Therefore, landform nesting between stages cannot be explained by landform relative abundances alone. This supports the notion that nested stage-dependent fluvial landforms are not independent of each other. In all river types, the most strongly overrepresented nesting structure is one where landform designation remains constant at all three stages. We found that for all river types baseflow nozzles are preferentially nested within bankfull wide bars, which supports the

expectations of flow convergence routing theory. We also found that wide bars are ubiquitously preferentially nested within oversized rectangles in both flow-stage nestings. Additionally, unconfined and partly confined river types 1, 2, and 5, had baseflow oversized rectangles preferentially nested within bankfull constricted pools. This preferential nesting structure was observed as well in river type 5 (Figure 11b) going from bankfull-to-flood stage, potentially contributing to the class's riffle-pool morphology. However, broadly our hypothesis that bankfull to flood-stage preferential nesting structures would be limited to river types 3 and 5 was incorrect.
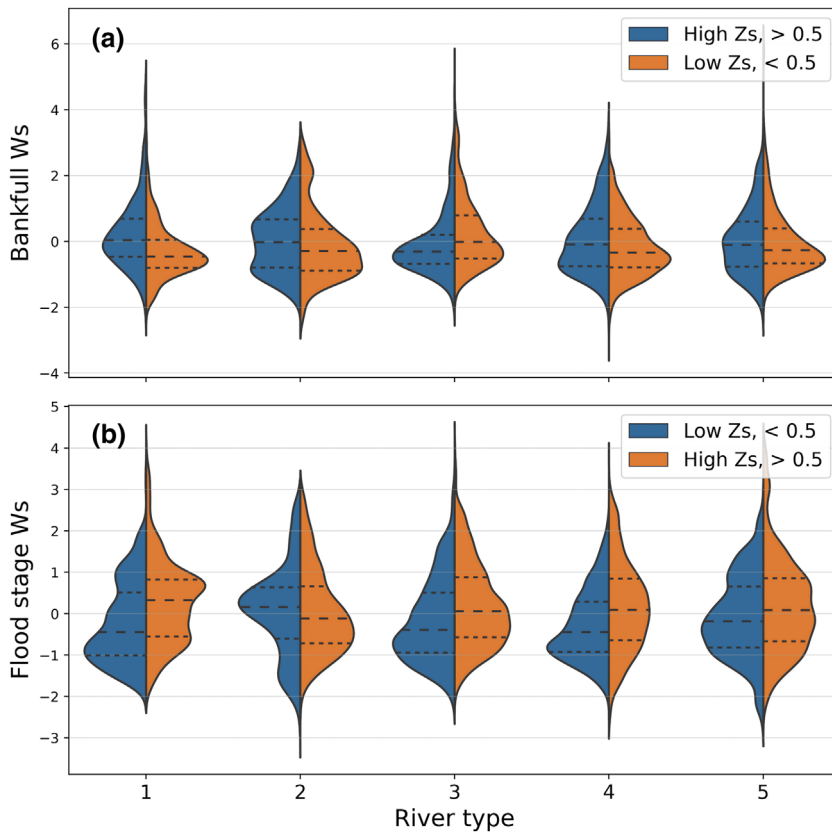
FIGURE 10 Violin plots addressing Question O2a by showing the distributions of width values at bankfull (A) and flood-stage (B) associated with topographic highs and lows at baseflow and bankfull respectively. Median indicated with long dash line, 25th and 75th quartiles indicated with short dash lines. See Table 1 for river type descriptions.

A handful of river type-specific preferred nesting structures were observed as well. River type 1 (Figure 11a) baseflow nozzle rectangles were preferentially nested within bankfull wide bars. Bankfull constricted pools are preferentially nested within flood stage nozzles at more than twice the expected frequency. In addition, river type 2 bankfull nozzles were preferentially nested within flood stage constricted pools and vice-versa, with constricted pools at bankfull preferentially nested within flood stage nozzles.

6 | DISCUSSION

Flow convergence routing is a relatively young theory for which only a few studies directly address it, and most past studies have focused on riffle-pool river types, except Pasternack et al. (2021). MacWilliams et al. (2006) re-interpreted 19 past field studies considering this mechanism but did not attempt a systematic analysis of the influence of river type and climate. Most recently, Byrne et al. (2021) investigated an entire region for its presence/absence of velocity reversals in riffle-pool channels, which are a simplified, two-stage expression of flow convergence routing in just one river type. They found that among 702 pool-riffle couplets, only 18% met the criteria to have a velocity reversal. Where velocity reversals occur, the channel was unusually different in its bankfull width than the reach-average width, which is what identified that width was the driving cause in these locations. Further, they then found that velocity reversal pools were almost always (89%) associated with channel constrictions while riffles were typically (71%) associated with channel expansions. Consequently, most of what is known comes from studies of this mechanism in gravel and cobble bedded streams in temperate and semiarid partly confined rivers (Gervasi et al., 2021; Sawyer et al., 2010; White

et al., 2010). This study sought to significantly broaden the range of river types for which flow convergence routing has been investigated, though still leaving many more types yet to be explored, such as in periglacial, temperate, and tropical climates.

Among the numerous interesting results from answering five specific questions using data from 35 river reach, the discussion necessarily focuses on the most important, novel scientific findings of the study. Specifically, how flow convergence routing theory applies to five river types in a less-studied but globally important climate. Climate change is anticipated to expand aridity, making the understanding of these rivers of greater importance to the future of river management. The discussion is organized by river confinement. Four other meaningful topics are addressed in the Supplementary Material file: major sources of uncertainty, expanding the scope of GCS analysis, investigating underlying factors supporting width variability, and moving beyond river type classification.

6.1 | Unconfined ephemeral river types

On average, we found that ephemeral rivers in unconfined corridors have Ws and Zs longitudinal patterning at bankfull that strongly match the predictions of flow convergence routing theory in a two-stage mode. Unlike partly confined (types 2 and 5) and confined (types 3 and 4) river types, unconfined river type 1 Ws and Zs series do not covary coherently (Table 3) at either baseflow or flood-stage. The lack of such coherence at flood stage was predicted; in an unconfined setting, floodplain, terrace, or valley hillside width undulation would primarily steer flow in a highly dispersed state (given the high cross-sectional area) with little channel-altering potential. That is not to say that during larger floods the effective width with fractional discharge
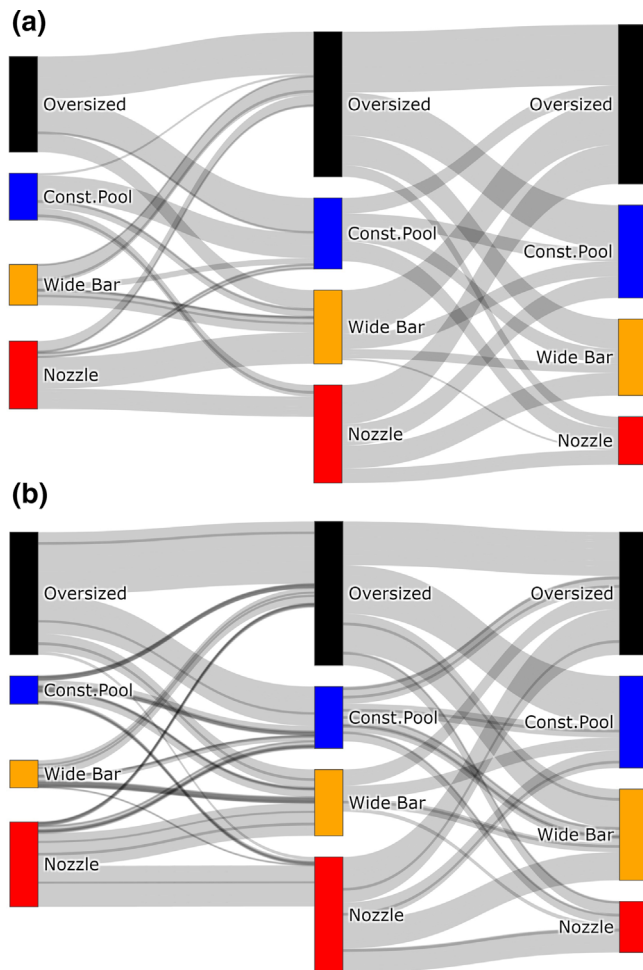
(a)

(b)

FIGURE 11 Selected Sankey diagrams address Question O2b by visually representing abundances of specific landforms nesting (excluding normal) for all sites in river type 1 (A) and all sites in river type 5 (B). Left, middle, and right columns depict baseflow, bankfull, and flood water stages, respectively.

over the channel itself (as opposed to the flow over floodplains and terraces) is not continuing to influence sediment transport and bankfull channel change, but simply that such changes are not strongly influenced by topographic undulations at the far lateral extent of the wetted area during a flood. In contrast, at bankfull stage unconfined reaches have a high bankfull mean C (Ws, Zs) value of 0.38, with on average more than 60% of rectangles having positive Ws·Zs covariance (Table 3). This suggests that flow convergence routing plays a dominant role at bankfull discharge exclusively and self-organizes longitudinal fluvial topography without confining valley input. In addition, baseflow topographic highs and lows (see question O2a) are more strongly associated with bankfull wide and narrow intervals, respectively, than in any other river type in this study (Figure 10). We conclude that in unconfined settings bankfull scale width undulations largely control in-channel sedimentary dynamics via the flow convergence routing mechanism. Note that bed undulations cannot control width undulations, because there is no mechanism by which deep pools can cause channels to constrict, the way that constrictions can cause beds to scour into deep pools (more explanation in the Supplementary Material File question O2a hypothesis narrative).

Although there is no basis for comparison with the literature on channel landforms in ephemeral streams, this conclusion is consistent

with findings from past studies of riffle-pool streams in a two-stage topographic setting, including both field studies and flume experiments investigating flow, sediment dynamics, and in-channel landforms in a channel with imposed bankfull width undulations (Chartrand et al., 2018; Nelson et al., 2015). For example, Hassan et al. (2021) tracked conditions through time in the field and in a flume. They found that major width constrictions drove the formation of pool-riffle couplets and that channel width variation was a primary control on bed undulation.

6.2 | Partly confined ephemeral river types

In evaluating flow convergence routing across five river types with ephemeral hydrology, the theory is largely supported by our sample of partly confined, riffle-pool river reaches (types 2 and 5). The study reaches typically switch dramatically from having negative covariance baseflow GCS, to positive covariance bankfull GCS (see question O1a). Mean C (Ws, Zs) shifts from −0.35 at baseflow to 0.28 at bankfull, a statistically significant increase of 0.63. In contrast, partially confined river type 2 has a similar mean bankfull C (Ws, Zs) value but experiences a much smaller, non-statistically significant 0.35 increase in mean C (Ws, Zs), because it was already higher than for other river types. This suggests that while bankfull width appears to somewhat control channel bed elevation in partly confined rivers broadly (consistent with the literature, e.g. Chartrand et al., 2018), riffle-pool channel morphology may specifically be a product of the observed Ws·Zs covariance sign reversal going from baseflow to bankfull. In other words, it is possible that bankfull geometry with coherent, in-phase width and bed elevation undulations coalesces all together when alluvial landforms re-organize, driven by flow convergence routing during floods of sufficient duration or repetition to re-organize a reach, as evidenced by the presence of positive covariance bankfull GCS.

While the origin of bankfull geometry may be a mutual coalescence of width and bed undulations, that of baseflow geometry involves width control over bed undulations. Using landform rectangular area as a proxy for velocity in our landform nesting analysis (see question O2b), we can see that flow convergence routing theory's prediction is supported. That is, baseflow nozzles (flow convergence, high velocity) are preferentially nested within bankfull wide bars (flow divergence, low velocity), and baseflow oversized rectangles (flow divergence, low velocity) are preferentially nested within bankfull constricted pools (flow convergence, high velocity). There is no morphodynamic mechanism in which baseflow morphology drives larger scale bankfull geometry, so the direction of causality is deductible. River type 5's preferential landform nesting structure is visualized using a Sankey diagram (Figure 11b). The strong association and the available morphodynamic mechanisms lead to the conclusion that bankfull channel width undulations, given suitable sediment supply, can topographically steer bankfull hydraulics and likely influence the hydraulics for the effective width of partial discharge over the channel during small floods, thereby maintaining bed relief with positive C (Ws,Zs).

We cannot ascertain which water stages are dominating the process in collaboration with bankfull channel topography. It is possible that bankfull flow is sufficient, though Shields stress evaluations have cast doubt on that for gravel and cobble bedded rivers (Pasternack

et al., 2018b, 2021). It is also possibility that flood flows control both baseflow and bankfull topography simultaneously. Finally, it is possible that flood flows control bankfull topography at flood peaks, and then on the falling limb bankfull topography drives topographic steering and morphodynamics of the nested baseflow topography. Detailed hydrodynamic and morphodynamic studies are needed to continue to investigate these possibilities (Sawyer et al., 2010; Strom et al., 2016). Recent studies have evaluated not only the discharges driving morphodynamics, but the more complex dynamics involving unsteady flows and the sequencing of floods (e.g., Vahidi et al., 2020).

6.3 | Confined ephemeral river types

Valley confined river reaches have been previously characterized by a "Pool Expansion Riffle Contraction" (PERC) configuration, which describes a setting where narrow cross-sections tend to be shallow, and wide cross-sections tend to be deep (Datry et al., 2017; Movahedi et al., 2021). This pattern can hold across a wide range of stages (Pasternack et al., 2021). Generally, the configuration's counter-intuitive stability is not self-generated by internal dynamics but rather imposed by width-restricting, elevation-increasing hillslope debris flows, resistant bedrock outcrops, tributary fan deposits, and the scour potential associated with large boulders (Datry et al., 2017; Kieffer, 1989).

We find with ephemeral hydrology that this traditional characterization of valley-confined longitudinal topography exists predominantly at baseflow and is altered as stage increases. In both confined river types (river types 3 and 4), mean C (Ws, Zs) at baseflow is strongly negative (Table 3) and there is a high relative abundance of nozzle and oversized landforms (Figure 9). The baseflow bivariate Ws, Zs distributions (Figure 8) visualize the skew towards negative Ws-Zs covariance, and for river type 3 specifically, display a surprising level of 2D organization given the volume of rectangles studied (see question O1b). In contrast to other river types where flood stage mean C (Ws, Zs) is comparable or less than bankfull, in confined settings mean C (Ws, Zs) increases with stage. Despite this, the PERC configuration description of mountain rivers (Movahedi et al., 2021), as represented here by negative C (Ws, Zs), generally ignores the flow-dependent nature of confined setting fluvial topography. This may be related to the difficulty of gathering field data in confined mountain rivers at flashy high flows, and potentially is an example of how meter-resolution topo-bathymetric DEMs can contribute to our broadly fieldwork-based understanding of fluvial geomorphology.

Our analysis suggests that in contrast to other river types, in the valley-confined river types, flow convergence routing's relevance as a morphodynamic mechanism is broadly limited to and depends on large floods (e.g., >50-year recurrence). Bankfull inundated topography appears to exist in a transitory state between negative and positive C (Ws, Zs) channel configurations (Table 3), and in river type 3 specifically, has no relationship to baseflow bed elevation undulations (see question O2a). At flood stage, both confined river types have positive mean C (Ws, Zs) values (Table 3), with the percent of rectangles on average with positive Ws-Zs covariance near 60%.

We notice that the described baseflow-to-flood stage increase in mean C (Ws, Zs) is of significantly greater magnitude, and occurring at higher stages, for river type 3 than river type 4. This strongly suggests

that, as hypothesized, sediment size plays a key role in determining at what discharge flow convergence routing begins to define channel dimensions (Bayat et al., 2017; Jackson et al., 2015). Rivers of type 3 and 4 all exist in South Coast mountains, which are characterized by high volumes of episodically supplied, poorly sorted, sediment driven by colluvial hillslope processes (Inman & Jenkins, 1999).

In a hypothetical setting with a uniform sediment size distribution, flow convergence routing could suddenly become relevant above the specific discharge capable of mobilizing said sediment size, but to significantly alter landforms it would take more than that. In such a case, we would expect to see channel topography favoring positive C (Ws, Zs). Yet in our confined river reaches, especially ones with cobble-boulder sediment regimes (river type 3), we do not see such threshold-like behavior as was found for Pasternack et al. (2021). One possible explanation is the use of only three Zd stages in this study, whereas Pasternack et al. (2021) used seven, of which four were flood stages. Alternately, it could be more related to the very high sediment supply and flashy flow regime of South Coast ephemeral streams in California, compared with the high-elevation, high precipitation setting of Pasternack et al. (2021). Therefore, in reaches with high fluxes of very coarse sediment, flow convergence routing may become more relevant as flood stage rises further. Another possibility is that a confining valley wall's ability to drive sedimentary dynamics is inversely proportional to its distance from the thalweg, because a proximal valley wall steers flow that is less laterally dispersed, and therefore at higher energy state. In conclusion, valley-confined river baseflow channels with ephemeral hydrology can broadly be characterized by the negative C (Ws, Zs). Yet larger scale sedimentary dynamics appear to require and be driven by the highest discharges via flow convergence routing (Pasternack et al., 2021), potentially as a function of the sediment size distribution or lateral distance to valley/canyon walls.

6.4 | Management significance

Applying our findings to a flow regulation context, we suggest that releasing bankfull discharge flows is necessary to maintain riffle-pool habitat, with the specific duration required up for local determination. In a river restoration design context, our findings suggest that in non-mountainous settings constructing resilient bankfull scale width undulation is likely to induce freely forming in-channel bed undulations. In mountainous settings however, our findings suggest that constructing additional resilient over-bank width undulations is likely also necessary to free form in-channel bed undulations. Additionally, we provide a proof-of-concept for future high-resolution DEM-based, larger sample size, fluvial geomorphology research at regional to global scales.

7 | CONCLUSIONS

To assess whether a large sample of ephemeral river reaches exhibit geomorphic differences between river types and as a function of stage, we generated 35 m-scale resolution topo-bathymetric DEMs of morphologically diverse ephemeral river reaches in the South Coast region of California. Broadly, we found that geomorphic covariance analysis applied regionally can help identify the role of a specific hydro-morphodynamic mechanism in different river types. GCS

methodology produces longitudinal standardized width and standardized, detrended bed elevation series at three key water stages. We analyzed these series to interpret fluvial topography in relation to flow convergence routing. We found that all river types have longitudinal fluvial topographic structures that significantly differ across three key water stages, which in some cases facilitated coherent hydromorphodynamic interpretations.

ACKNOWLEDGMENTS

DATA AVAILABILITY STATEMENT

This study only used free, publicly available airborne lidar data that all came from the public website OpenTopography (https://opentopography.org). The algorithm for processing the lidar data used in this study is free and publicly available at https://gcs-gui-documentation.readthedocs.io/.

ORCID

Gregory B. Pasternack 🔟 https://orcid.org/0000-0002-1977-4175

Belize A. Lane 🔟 https://orcid.org/0000-0003-2331-7038

REFERENCES

Abatzoglou, J.T., Redmond, K.T. & Edwards, L.M. (2009) Classification of regional climate variability in the state of California. *Journal of Applied Meteorology and Climatology*, 48(8), 1527–1541. Available from: https://doi.org/10.1175/2009JAMC2062.1

Adams, D.L. (2020) Toward bed state morphodynamics in gravel-bed rivers. *Progress in Physical Geography: Earth and Environment*, 44(5), 700–726. Available from: https://doi.org/10.1177/0309133320900924

Annis, A., Nardi, F., Morrison, R.R. & Castelli, F. (2019) Investigating hydrogeomorphic floodplain mapping performance with varying DTM resolution and stream order. *Hydrological Sciences Journal*, 64(5), 525–538. Available from: https://doi.org/10.1080/02626667.2019.1591623

Baartman, J.E.M., Masselink, R., Keesstra, S.D. & Temme, A.J.A.M. (2013) Linking landscape morphological complexity and sediment connectivity. *Earth Surface Processes and Landforms*, 38(12), 1457–1471. Available from: https://doi.org/10.1002/esp.3434

Bayat, E., Rodríguez, J.F., Saco, P.M., De Almeida, G.A., Vahidi, E. & García, M.H. (2017) A tale of two riffles: using multidimensional, multifractional, time-varying sediment transport to assess self-maintenance in pool-riffle sequences. *Water Resources Research*, 53(3), 2095–2113. Available from: https://doi.org/10.1002/2016WR019464

Billi, P., Demissie, B., Nyssen, J., Moges, G. & Fazzini, M. (2018) Meander hydromorphology of ephemeral streams: similarities and differences with perennial rivers. *Geomorphology*, 319, 35–46. Available from: https://doi.org/10.1016/j.geomorph.2018.07.003

Brown, R.A. & Pasternack, G.B. (2014) Hydrologic and topographic variability modulate channel change in mountain rivers. *Journal of Hydrology*, 510, 551–564. Available from: https://doi.org/10.1016/j.jhydrol.2013.12.048

Brown, R.A. & Pasternack, G.B. (2017) Bed and width oscillations form coherent patterns in a partially confined, regulated gravel-cobble-bedded river adjusting to anthropogenic disturbances. *Earth Surface Dynamics*, 5(1), 1–20. Available from: https://doi.org/10.5194/esurf-5-1-2017

Brown, R.A., Pasternack, G.B. & Lin, T. (2015) The topographic design of river channels for form-process linkages for river restoration. *Environmental Management*, 57(4), 929–942. Available from: https://doi.org/10.1007/s00267-015-0648-0

Brown, R.A., Pasternack, G.B. & Wallender, W.W. (2014) Synthetic river valleys: creating prescribed topography for form-process inquiry and river rehabilitation design. *Geomorphology*, 214, 40–55. Available from: https://doi.org/10.1016/j.geomorph.2014.02.025

Bull, L.J., Kirkby, M.J., Shannon, J. & Hooke, J.M. (2000) The impact of rainstorms on floods in ephemeral channels in Southeast Spain. *Catena*, 38(3), 191–209. Available from: https://doi.org/10.1016/S0341-8162(99)00071-5

Byrne, C.F., Guillon, H., Lane, B.A., Pasternack, G.B. & Sandoval-Solis, S. (2020) *Coastal California regional geomorphic classifications*. Sacramento, CA: California State Water Resources Control Board.

Byrne, C.F., Pasternack, G.B., Guillon, H., Lane, B.A. & Sandoval-Solis, S. (2021). Channel constriction predicts pool-riffle velocity reversals across landscapes. *Geophysical Research Letters*, 48, e2021GL094378. Available from: https://doi.org/10.1029/2021GL094378

Caamaño, D., Goodwin, P., Buffington, J.M., Liou, J.C.P. & Daley-Laursen, S. (2009) Unifying criterion for the velocity reversal hypothesis in gravel-bed rivers. *Journal of Hydraulic Engineering*, 135(1), 66–70. Available from: https://doi.org/10.1061/(ASCE)0733-9429(2009)135:1(66

Carling, P.A. (1991) An appraisal of the velocity-reversal hypothesis for stable pool-riffle sequences in the river Severn, England. *Earth Surface Processes and Landforms*, 16(1), 19–31. Available from: https://doi.org/10.1002/esp.3290160104

Carson, M.A. (1984) The meandering-braided river threshold: a reappraisal. *Journal of Hydrology*, 73(3–4), 315–334. Available from: https://doi.org/10.1016/0022-1694(84)90006-4

Cavalli, M., Tarolli, P., Marchi, L. & Dalla Fontana, G. (2008) The effectiveness of airborne LiDAR data in the recognition of channel-bed morphology. *Catena*, 73(3), 249–260. Available from: https://doi.org/10.1016/j.catena.2007.11.001

Chartrand, S.M., Jellinek, A.M., Hassan, M.A. & Ferrer-Boix, C. (2018) Morphodynamics of a width-variable gravel bed stream: new insights on pool-riffle formation from physical experiments. *Journal of Geophysical Research - Earth Surface*, 123(11), 2735–2766. Available from: https://doi.org/10.1029/2017JF004533

Clubb, F.J., Mudd, S.M., Milodowski, D.T., Valters, D.A., Slater, L.J., Hurst, M.D., et al. (2017) Geomorphometric delineation of floodplains and terraces from objectively defined topographic thresholds. *Earth Surface Dynamics*, 5(3), 369–385. Available from: https://doi.org/10.5194/esurf-5-369-2017

Datry, T., Bonada, N. & Boulton, A.J. (2017) Chapter 1 - General Introduction. In: Datry, T., Bonada, N. & Boulton, A. (Eds.) *Intermittent Rivers Ephemeral streams*. London, UK: Academic Press, pp. 21–49. https://doi.org/10.1016/B978-0-12-803835-2.00002-4

David, S.R., Edmonds, D.A. & Letsinger, S.L. (2017) Controls on the occurrence and prevalence of floodplain channels in meandering rivers. *Earth Surface Processes and Landforms*, 42(3), 460–472. Available from: https://doi.org/10.1002/esp.4002

De Almeida, G.A.M. & Rodríguez, J.F. (2012) Spontaneous formation and degradation of pool-riffle morphology and sediment sorting using a simple fractional transport model. *Geophysical Research Letters*, 39(6), 1–7. Available from: https://doi.org/10.1029/2012GL051059

Dettinger, M.D., Ralph, F.M., Das, T., Neiman, P.J. & Cayan, D.R. (2011) Atmospheric rivers, floods and the water resources of California. *Watermark*, 3(2), 445–478. Available from: https://doi.org/10.3390/w3020445

Diplas, P., Dancey, C.L., Celik, A.O., Valyrakis, M., Greer, K. & Akar, T. (2008) The role of impulse on the initiation of particle movement under turbulent flow conditions. *Science*, 322(5902), 717–720. Available from: https://doi.org/10.1126/science.1158954

Duffin, J., Carmichael, R.A., Yager, E.M., Benjankar, R. & Tonina, D. (2021) Detecting multi-scale riverine topographic variability and its influence on Chinook salmon habitat selection. *Earth Surface Processes and Landforms*, 46(5), 1026–1040. Available from: https://doi.org/10.1002/esp.5077

Eaton, B.C., Millar, R.G. & Davidson, S. (2010) Channel patterns: braided, anabranching, and single-thread. *Geomorphology*, 120(3–4), 353–364. Available from: https://doi.org/10.1016/j.geomorph.2010.04.010

Erskine, W.D. & Livingstone, E.A. (1999) In-channel benches: the role of floods in their formation and destruction on bedrock confined rivers. In: Miller, A.J. & Gupta, A. (Eds.) *Varieties of fluvial form*. New York: John Wiley and Sons, pp. 445–475.

Fernandez Luque, R. & Van Beek, R. (1976) Erosion and transport of bed-load sediment. *Journal of Hydraulic Research*, 14(2), 127–144. Available from: https://doi.org/10.1080/00221687609499677

Gervasi, A.A., Pasternack, G.B. & East, A.E. (2021) Flooding duration and volume more important than peak discharge in explaining 18 years of gravel-cobble river change. *Earth Surface Processes and Landforms*, 46(15), 3194–3212. Available from: https://doi.org/10.1002/esp.5230

Gray, A.B., Pasternack, G.B., Watson, E.B., Warrick, J.A. & Goni, M.A. (2015) The effect of El Nino southern oscillation cycles on the decadal scale suspended sediment behavior of a coastal dry-summer subtropical catchment. *Earth Surface Processes and Landforms*, 40(2), 272–284. Available from: https://doi.org/10.1002/esp.3627

Gray, A.B., Pasternack, G.B., Watson, E.B., Warrick, J.A. & Goñi, M.A. (2015) Effects of antecedent hydrologic conditions, time dependence, and climate cycles on the suspended sediment load of the Salinas River, California. *Journal of Hydrology*, 525, 632–649. Available from: https://doi.org/10.1016/j.jhydrol.2015.04.025

Guillon, H., Byrne, C.F., Lane, B.A., Sandoval Solis, S. & Pasternack, G.B. (2020) Machine learning predicts reach-scale river types from coarse-scale geospatial data in a large river basin. *Water Resources Research*, 56(3), 1–22. Available from: https://doi.org/10.1029/2019WR026691

Hassan, M.A., Radić, V., Buckrell, E., Chartrand, S.M. & McDowell, C. (2021) Pool-riffle adjustment due to changes in flow and sediment supply. *Water Resources Research*, 57(2), e2020WR028048. Available from: https://doi.org/10.1029/2020WR028048

Hill, R.A., Marc, H.W., Scott, G.L., Anthony, R.O. & Darren, J.T. (2016) The stream-catchment (StreamCat) dataset: a database of watershed metrics for the conterminous United States. *Journal of the American Water Resources Association (JAWRA)*, 52(1), 120–128. Available from: https://doi.org/10.1111/1752-1688.12372

Hocini, N., Payrastre, O., Bourgin, F., Gaume, E., Davy, P., Lague, D., et al. (2020) Performance of automated flood inundation mapping methods in a context of flash floods: a comparison of three methods based either on the height above nearest drainage (HAND) concept, or on 1D/2D shallow water equations. *Hydrology and Earth System Sciences Discussions*, 10, 5194.

Hooke, J.M. (2016) Morphological impacts of flow events of varying magnitude on ephemeral channels in a semiarid region. *Geomorphology*, 252, 128–143. Available from: https://doi.org/10.1016/j.geomorph.2015.07.014

Hug, C., Krzystek, P. & Fuchs, W. (2004) Advanced LiDAR data processing with LasTools. In: *Proceedings of the XXth ISPRS Congress, 12-23 July 2004, Instabul, Turkey*. International Archives of the Photogrammetry, Remote Sensing and Spatial Information Sciences - ISPRS Archives, Vol.35, pp. 832–837. Available from:https://www.isprs.org/proceedings/XXXV/congress/comm2/papers/240.pdf

Inman, D.L. & Jenkins, S.A. (1999) Climate change and the episodicity of sediment flux of small California rivers. *Journal of Geology*, 107(3), 251–270. Available from: https://doi.org/10.1086/314346

Jackson, W.L. & Beschta, R.L. (1982) A model of two-phase bedload transport in an Oregon coast range stream. *Earth Surface Processes and Landforms*, 7(6), 517–527. Available from: https://doi.org/10.1002/esp.3290070602

Jackson, J.R., Pasternack, G.B. & Wheaton, J.M. (2015) Virtual manipulation of topography to test potential pool–riffle maintenance mechanisms. *Geomorphology*, 228, 617–627. Available from: https://doi.org/10.1016/j.geomorph.2014.10.016

Kasprak, A., Hough-Snee, N., Beechie, T., Bouwes, N., Brierley, G., Camp, R., et al. (2016) The blurred line between form and process: a comparison of stream channel classification frameworks. *PLoS ONE*, 11(3), e0150293. Available from: https://doi.org/10.1371/journal.pone.0150293

Keller, E.A. (1971) Areal sorting of bed-load material: the hypothesis of velocity reversal. *Bulletin of the Geological Society of America*, 82(3), 753–756. Available from: https://doi.org/10.1130/0016-7606(1971)82[753:ASOBMT]2.0.CO;2

Kieffer, S.W. (1985) The 1983 hydraulic jump in crystal rapid: implications for river-running and geomorphic evolution in the grand canyon. *The Journal of Geology*, 93(4), 385–406. Available from: https://doi.org/10.1086/628962

Kieffer, S.W. (1989) Geologic nozzles. *Reviews of Geophysics*, 27(1), 3–38. Available from: https://doi.org/10.1029/RG027i001p00003

Lague, D. & Feldmann, F. (2020) Chapter 2 -Topo-bathymetric airborne LiDAR for fluvial-geomorphology analysis. In: Tarolli, P. & Mudd, S.M. (Eds.) *Remote sensing of geomorphology*, Developments in Earth Surface Processes, Vol. 23. Amsterdam, Netherlands: Elsevier, pp. 5–54 https://doi.org/10.1016/B978-0-444-64177-9.00002-3

Lane, B.A., Guillon, H., Byrne, C.F., Pasternack, G.B., Rowles, J. & Sandoval-Solis, S. (2021) Channel reach morphology and landscape properties are linked across a large heterogeneous region. *Earth Surface Processes and Landforms*, 47(1), 257–274. Available from: https://doi.org/10.1002/esp.5246

Lane, B.A., Sandoval-Solis, S., Stein, E.D., Yarnell, S., Pasternack, G.B. & Dahlke, H. (2018) Beyond metrics: the role of hydrologic baseline archetypes in environmental water management. *Environmental Management*, 62(4), 678–693. Available from: https://doi.org/10.1007/s00267-018-1077-7

Lindroth, E.M., Rhoads, B.L., Castillo, C.R., Czuba, J.A., Güneralp, İ. & Edmonds, D. (2020) Spatial variability in bankfull stage and bank elevations of lowland meandering rivers: relation to rating curves and channel planform characteristics. *Water Resources Research*, 56(8), e2020WR027477. Available from: https://doi.org/10.1029/2020WR027477

Lowry, R. (2017) Chapter 8 - Chi-Square procedures for the analysis of categorical frequency data. In: *Concepts and applications of inferential statistics*. Poughkeepsie, NY, USA: Vassar College. Available at: https://web.archive.org/web/20171022032306/http://vassarstats.net:80/textbook/ch8pt1.html

MacWilliams, M.L., Wheaton, J.M., Pasternack, G.B., Street, R.L. & Kitanidis, P.K. (2006) Flow convergence routing hypothesis for pool-riffle maintenance in alluvial rivers. *Water Resources Research*, 42(10), 1–21. Available from: https://doi.org/10.1029/2005WR004391

Mahdade, M., Moine, N.L. & Moussa, R. (2018) Wavelet and index methods for the identification of pool–riffle sequences. *Hydrology and Earth System Sciences*, 24(7), 3513–3537. Available from: https://doi.org/10.5194/hess-24-3513-2020

Mann, H.B. & Whitney, D.R. (1947) On a test of whether one of two random variables is stochastically larger than the other. *The Annals of Mathematical Statistics*, 18(1), 50–60. Availablie from: https://doi.org/10.1214/aoms/1177730491

McJannet, D., Marvanek, S., Kinsey-Henderson, A., Petheram, C. & Wallace, J. (2014) Persistence of in-stream waterholes in ephemeral rivers of tropical northern Australia and potential impacts of climate change. *Marine and Freshwater Research*, 65(12), 1131–1144. Available from: https://doi.org/10.1071/MF14035

McKay, L., Bondelid, T., Dewald, T., Johnston, J., Moore, R. & Rea, A. (2012) Nhdplus version 2: User guide. [Computer software manual].

Merritt, A.M., Lane, B. & Hawkins, C.P. (2021) Classification and prediction of natural streamflow regimes in arid regions of the USA. *Watermark*, 13(3), 380. Available from: https://doi.org/10.3390/w13030380

Milan, D.J. & Schwendel, A.C. (2021) Climate-change driven increased flood magnitudes and frequency in the British uplands: geomorphologically informed scientific underpinning for upland flood-risk management. *Earth Surface Processes and Landforms*, 46(15), 3026–3044. Available from: https://doi.org/10.1002/esp.5206

Motta, D., Abad, J.D., Langendoen, E.J. & Garcia, M.H. (2012) A simplified 2D model for meander migration with physically-based bank evolution. *Geomorphology*, 163, 10–25. Available from: https://doi.org/10.1016/j.geomorph.2011.06.036

Movahedi, N., Dehghani, A.A., Schmidt, C., Trauth, N., Pasternack, G.B., Stewardson, M.J., et al. (2021) Hyporheic exchanges due to channel bed and width undulations. *Advances in Water Resources*, 149-(September 2020), 103857. Available from: https://doi.org/10.1016/j.advwatres.2021.103857

Nardini, A., Yépez, S., Mazzorana, B., Ulloa, H., Bejarano, M.D. & Laraque, A. (2020) A systematic, automated approach for river segmentation tested on the Magdalena River (Colombia) and the Baker River (Chile). *Watermark*, 12(10), 2827. Available from: https://doi.org/10.3390/w12102827

Nelson, P.A., Brew, A.K. & Morgan, J.A. (2015) Morphodynamic response of a variable-width channel to changes in sediment supply. *Water Resources Research*, 51(7), 5717–5734. Available from: https://doi.org/10.1002/2014WR016806

Nobre, A.D., Cuartas, L.A., Hodnett, M., Rennó, C.D., Rodrigues, G., Silveira, A., et al. (2011) Height above the nearest drainage–a hydrologically relevant new terrain model. *Journal of Hydrology*, 404(1–2), 13–29. Available from: https://doi.org/10.1016/j.jhydrol.2011.03.051

Notebaert, B., Verstraeten, G., Govers, G. & Poesen, J. (2009) Qualitative and quantitative applications of LiDAR imagery in fluvial geomorphology. *Earth Surface Processes and Landforms*, 34(March), 217–231. Available from: https://doi.org/10.1002/esp.1705

Passalacqua, P., Belmont, P., Staley, D.M., Simley, J.D., Arrowsmith, J.R., Bode, C.A., et al. (2015) Analyzing high resolution topography for advancing the understanding of mass and energy transfer through landscapes: a review. *Earth-Science Reviews*, 148, 174–193. Available from: https://doi.org/10.1016/j.earscirev.2015.05.012

Pasternack, G.B. (2011) *2D modeling and ecohydraulic analysis*. Createspace: Seattle, WA.

Pasternack, G.B., Baig, D., Weber, M.D. & Brown, R.A. (2018a) Hierarchically nested river landform sequences. Part 1: theory. *Earth Surface Processes and Landforms*, 43(12), 2510–2518. Available from: https://doi.org/10.1002/esp.4411

Pasternack, G.B., Baig, D., Weber, M.D. & Brown, R.A. (2018b) Hierarchically nested river landform sequences. Part 2: bankfull channel morphodynamics governed by valley nesting structure. *Earth Surface Processes and Landforms*, 43(12), 2519–2532. Available from: https://doi.org/10.1002/esp.4410

Pasternack, G.B., Gore, J. & Wiener, J. (2021) Geomorphic covariance structure of a confined mountain river reveals landform organization stage threshold. *Earth Surface Processes and Landforms*, 46(13), 2582–2606. Available from: https://doi.org/10.1002/esp.5195

Perignon, M., Adams, J., Overeem, I. & Passalacqua, P. (2020) Dominant process zones in a mixed fluvial–tidal delta are morphologically distinct. *Earth Surface Dynamics*, 8(3), 809–824. Available from: https://doi.org/10.5194/esurf-8-809-2020

Piegay, H., Mathias Kondolf, G., Toby Minear, J. & Vaudor, L. (2015) Trends in publications in fluvial geomorphology over two decades: a truly new era in the discipline owing to recent technological revolution? *Geomorphology*, 248, 489–500. Available from: https://doi.org/10.1016/j.geomorph.2015.07.039

Polade, S.D., Gershunov, A., Cayan, D.R., Dettinger, M.D. & Pierce, D.W. (2017) Precipitation in a warming world: assessing projected hydroclimate changes in California and other Mediterranean climate regions. *Scientific Reports*, 7(1), 10783. Available from: https://doi.org/10.1038/s41598-017-11285-y

Powell, D.M. (2009) Dryland Rivers: Processes and Forms. In: Parsons, A.-J. & Abrahams, A.D. (Eds.) *Geomorphology of desert environments*. Dordrecht: Springer. https://doi.org/10.1007/978-1-4020-5719-9_12

Powell, D.M., Reid, I. & Laronne, J.B. (2001) Evolution of bed load grain size distribution with increasing flow strength and the effect of flow duration on the caliber of bed load sediment yield in ephemeral gravel bed rivers. *Water Resources Research*, 37(5), 1463–1474. Available from: https://doi.org/10.1029/2000WR900342

Priddy, C.L. & Clarke, S.M. (2020) The sedimentology of an ephemeral fluvial–aeolian succession. *Sedimentology*, 67(5), 2392–2425. Available from: https://doi.org/10.1111/sed.12706

Rathjens, H., Bieger, K., Chaubey, I., Arnold, J.G., Allen, P.M., Srinivasan, R., et al. (2016) Delineating floodplain and upland areas for hydrologic

models: a comparison of methods. *Hydrological Processes*, 30(23), 4367–4383. Available from: https://doi.org/10.1002/hyp.10918

Richards, K.S. (1976) Channel width and the riffle-pool sequence. *Geological Society of America Bulletin*, 87(6), 883–890. Available from: https://doi.org/10.1130/0016-7606(1976)87<883:CWATRS>2.0.CO;2

Roth, D.L., Doane, T.H., Roering, J.J., Furbish, D.J. & Zettler-Mann, A. (2020) Particle motion on burned and vegetated hillslopes. *Proceedings of the National Academy of Sciences of the United States of America*, 117(41), 25335–25343. Available from: https://doi.org/10.1073/pnas.1922495117

Sawyer, A.M., Pasternack, G.B., Moir, H.J. & Fulton, A.A. (2010) Riffle-pool maintenance and flow convergence routing observed on a large gravel-bed river. *Geomorphology*, 114(3), 143–160. Available from: https://doi.org/10.1016/j.geomorph.2009.06.021

Scown, M.W., Thoms, M.C. & De Jager, N.R. (2015) Floodplain complexity and surface metrics: influences of scale and geomorphology. *Geomorphology*, 245, 102–116. Available from: https://doi.org/10.1016/j.geomorph.2015.05.024

Segura-Beltran, F. & Sanchis-Ibor, C. (2013) Assessment of channel changes in a Mediterranean ephemeral stream since the early twentieth century. The Rambla de Cervera, eastern Spain. *Geomorphology*, 201, 199–214. Available from: https://doi.org/10.1016/j.geomorph.2013.06.021

Strom, M.A., Pasternack, G.B. & Wyrick, J.R. (2016) Reenvisioning velocity reversal as a diversity of hydraulic patch behaviors. *Hydrological Processes*, 30(13), 2348–2365. Available from: https://doi.org/10.1002/hyp.10797

Thornbury, W.B. (1954) Principles of geomorphology. Wiley, New York. 46(8), 392. Available from: https://doi.org/10.2134/agronj1954.00021962004600080009x

Tonina, D., McKean, J.A., Benjankar, R.M., Yager, E., Carmichael, R.A., Chen, Q., et al. (2020) Evaluating the performance of topobathymetric LiDAR to support multi-dimensional flow modelling in a gravel-bed mountain stream. *Earth Surface Processes and Landforms*, 45(12), 2850–2868. Available from: https://doi.org/10.1002/esp.4934

Tooth, S. (2000) Process, form and change in dryland rivers: a review of recent research. *Earth-Science Reviews*, 51(1–4), 67–107. Available from: https://doi.org/10.1016/S0012-8252(00)00014-3

Vahidi, E., Rodríguez, J.F., Bayne, E. & Saco, P.M. (2020) One flood is not enough: Pool-riffle self-maintenance under time-varying flows and nonequilibrium multifractional sediment transport. *Water Resources Research*, 56(8), e2019WR026818. Available from: https://doi.org/10.1029/2019WR026818

Warrick, J.A., Hatten, J.A., Pasternack, G.B., Gray, A.B., Goni, M.A. & Wheatcroft, R.A. (2012) The effects of wildfire on the sediment yield of a coastal California watershed. *Geological Society of America Bulletin*, 124(7–8), 1130–1146. Available from: https://doi.org/10.1130/B30451.1

Wheaton, J.M., Brasington, J., Darby, S.E., Kasprak, A., Sear, D. & Vericat, D. (2013) Morphodynamic signatures of braiding mechanisms as expressed through change in sediment storage in a gravel-bed river. *Journal of Geophysical Research - Earth Surface*, 118(2), 759–779. Available from: https://doi.org/10.1002/jgrf.20060

White, J.Q., Pasternack, G.B. & Moir, H.J. (2010) Valley width variation influences riffle-pool location and persistence on a rapidly incising gravel-bed river. *Geomorphology*, 121(3–4), 206–221. Available from: https://doi.org/10.1016/j.geomorph.2010.04.012

Wilson, C.A. & Goodbred, S.L., Jr. (2015) Construction and maintenance of the Ganges-Brahmaputra-Meghna delta: linking process, morphology, and stratigraphy. *Annual Review of Marine Science*, 7(1), 67–88. Available from: https://doi.org/10.1146/annurev-marine-010213-135032

Wohl, E. (2019) Forgotten legacies: understanding and mitigating historical human alterations of river corridors. *Water Resources Research*, 55(7), 5181–5201. Available from: https://doi.org/10.1029/2018WR024433

Wohl, E. & Pearthree, P. (1991) Debris flows as geomorphic agents in the Huachuca Mountains of southeastern Arizona. *Geomorphology*, 4(3–

4), 273–292. Available from: https://doi.org/10.1016/0169-555X(91)90010-8

Wohlgemuth, P.M., Beyers, J.L. & Conard, S.G. (1999) Postfire hillslope erosion in southern California chaparral: a case study of prescribed fire as a sediment management tool. *Proceedings of Symposium on Fire Economics, Planning and Policy: Bottom Lines*, 173, 269–276.

Wyrick, J.R. & Pasternack, G.B. (2016) Revealing the natural complexity of topographic change processes through repeat surveys and decision-tree classification. *Earth Surface Processes and Landforms*, 41(6), 723–737. Available from: https://doi.org/10.1002/esp.3854

Yager, E.M., Venditti, J.G., Smith, H.J. & Schmeeckle, M.W. (2018) The trouble with shear stress. *Geomorphology*, 323, 41–50. Available from: https://doi.org/10.1016/j.geomorph.2018.09.008

Yuen, K.K. (1974) The two-sample trimmed t for unequal population variances. *Biometrika*, 61(1), 165–170. Available from: https://doi.org/10.1093/biomet/61.1.165

Zheng, X., Tarboton, D.G., Maidment, D.R., Liu, Y.Y. & Passalacqua, P. (2018) River channel geometry and rating curve estimation using height above the nearest drainage. *Journal of the American Water Resources Association*, 54(4), 785–806. Available from: https://doi.org/10.1111/1752-1688.12661

SUPPORTING INFORMATION

Additional supporting information can be found online in the Supporting Information section at the end of this article.

How to cite this article: Nogueira, X.R., Pasternack, G.B., Lane, B.A. & Sandoval-Solis, S. (2024) Width undulation drives flow convergence routing in five flashy ephemeral river types across a dry summer subtropical region. *Earth Surface Processes and Landforms*, 1–24. Available from: https://doi.org/10.1002/esp.5805